Development of highly porous activated carbon by pressurized physical activation method and its application

李, 炫錫

加圧物理賦活法による

高細孔発達度活性炭の開発とその応用

Development of highly porous activated carbon by pressurized physical activation method and its application

2022年 3月

九州大学大学院

総合理工学府

量子プロセス理工学専攻

李　炫錫

Hyeonseok Yi

加圧物理賦活法による

高細孔発達度活性炭の開発とその応用

Development of highly porous activated carbon by pressurized physical activation method and its application

指導教員： 宮脇　仁

2022年 3月

九州大学大学院
総合理工学府
量子プロセス理工学専攻

李　炫錫

Hyeonseok Yi

論文調査委員会

主査 九州大学 准教授　宮脇　仁
副査 九州大学 教授　　尹　聖昊
副査 九州大学 教授　　宮崎　隆彦

Abstract

Activated carbon is an artificial carbon material that is usually produced from coal, petroleum, wood, resin, biomass and so on. Due to its developed pore structure, activated carbon exhibits a very high specific surface area and pore spaces of molecular dimension. Since such pores work as an adsorption site for various molecules and ions, activated carbons are used for purification of air and water, separation of gases, and as catalyst carrier or catalyst support. Also, activated carbons are widely used in energy storage devices such as electric double layer capacitors or Li-S cells.

Activation method is mainly divided into chemical activation and physical activation. For chemical activation, chemicals such as KOH, NaOH, and $ZnCl_2$ are used as activation agents, and chemically activated carbon having a high specific surface area and a relatively narrow pore size distribution can be produced in high yield by the catalytic reaction of metal ion. On the other hand, physical activation uses oxidation gas such as steam, CO_2, and air to introduce pore structure by gasification of the carbonized material. Although physical activation gives activated carbon with relatively low specific surface area and activation yield, it is possible to produce activated carbon at a low cost. Most of challenges about the activated carbon manufacturing is the development of a method for producing activated carbon at low cost such as physical activation, while having a high specific surface area and high yield like chemical activation.

In order to manufacture activated carbon with high pore development, it is necessary to improve the understanding of the pore structure of activated carbon. Unlike traditional pore models, our research group proposed a new pore structure model; hierarchical structure model based on microdomain. By increasing pore development degree, microdomain size was

decreased in pitch-based physically activated carbon fiber. Besides, in our previous study, we reported that the yield and pore development were lowered due to the lack of diffusibility of the activation agent onto carbon material in physical activation compared to chemical activation. Therefore, as a method to improve diffusibility of activation agent, we focused on pressurization during physical activation process.

In this thesis, we would like to suggest a new and facile method to produce activated carbon with high yield and pore development degree. In order to suggest the pressurized physical activation, the following factors should be considered;

(1) Effect of pressurization to yield and pore structure development

(2) Influence to the particle and microdomain structure

(3) Application and generalization

Abstracts of each chapter in this thesis are summarized as below;

In Chapter 3, we would like to establish a method for high yield and pore development degree of activated carbon by the pressurization. Firstly, we attempted to elucidate the effect of pressurization on the activated carbon yield, pore development degree and other factors. It was confirmed that the gasification, the main reaction of physical activation, is promoted by pressurization. Next, in order to investigate the effect of pressurization on particles, microdomain, and pore structure, activated carbon sample was prepared using MSB-TG and the pore development degree was evaluated. As a result, it was confirmed that when compared with the atmospheric physical activation condition, the specific surface area is significantly increased by pressurized physical activation. In addition, many large micropores were introduced by pressurization from the pore size distribution results. As a result of STM

observation, it was confirmed that the cause of the difference in the high specific surface area and the pore size distribution was due to the difference in the size and development of the microdomains between atmospheric and pressurized physical activation. However, since the morphology and particle size distribution of the activated carbon do not change significantly by pressurization, it means that the heterogeneous gasification reaction on the outer surface of the particles has been improved. Consequently, it was possible to confirm the effect and possibility of the pressurized physical activation method onto particle and microdomain.

In Chapter 4, we suggested "Pressurized physical activation" method for facile method having high yield and more development degree of activated carbon manufacturing process. Physical activation methods are commonly adopted in industry because of their low production costs, but the lack of activating agent diffusibility into core parts of the particles and microdomains of carbon materials causes a lower activation yield and degree of pore development, compared with chemical activation methods. To increase the diffusibility of activating agent into carbon material and corresponding degree of pore development, we propose a novel pressurized physical activation method. Pressurization showed remarkable increases in specific surface area and total pore volume of the prepared activated carbon, compared with atmospheric physical activation. Additionally, in activated carbon prepared by pressurization, pore size distribution analysis revealed characteristic development of micropores of about 1.6 nm; such micropores did not appear in activated carbon under conventional atmospheric physical activation. Furthermore, observations of particles and microdomains showed that pressurization increased the diffusibility of activation agent in carbon particles, but not at the microdomain level. This innovative pressurized physical activation can produce activated carbon with highly developed pores (specific surface area > 2,600 m^2/g) and a unique pore size distribution due to the improved activating agent diffusibility in carbon particle level.

In Chapter 5, we applied pressurized activated carbon as adsorbent for ethanol adsorption heat pump. Although chemically activated carbon with highly developed pore structures exhibits good ethanol adsorption performance, high activated carbon manufacturing costs inhibit its practical application as an adsorption heat pump adsorbent. Moreover, although physical activation can produce inexpensive activated carbon, the limited pore development limits the ethanol adsorption performance. Recently, we developed a pressurized physical activation method that can produce activated carbon with a well-developed pore structure and characteristic pore size distribution with relatively high yield. In this study, we investigated the applicability of the pressurized physically activated carbon as an adsorbent in activated carbon–ethanol type adsorption heat pump system. Because of the large proportions of appropriate size pores by pressurization, the pressurized physically activated carbon showed effective ethanol adsorption performance comparable with that of chemically activated carbon on a weight basis. Furthermore, on a volume basis, the pressurized physically activated carbon, with a high bulk density, showed much higher effective ethanol adsorption performance than chemically activated carbon. These results reveal the potential of the pressurized physically activated carbon as a relatively inexpensive high-performance adsorbent for AHP systems with ethanol refrigerant.

In Chapter 6, obtained results and discussions in this thesis were summarized as conclusion.

Contents

Chapter 1.

General introduction

1.1 Activated carbon

Recently, the need of porous materials has emerged as an advanced storage material such as the use of hydrogen energy and the medium for carrying gas. Activated carbon is one of useful artificial porous carbon materials that having a well-developed pore structure and high specific surface area among carbon materials [1]. Thus, activated carbon exhibit superior adsorption performance for various molecules and ions. Together with the porosity, surface functionality is also related to adsorption phenomena and performance. Adsorption is a phenomenon in which the concentration of molecules or ions on the solid surface is higher than the surroundings, and diffusion of adsorbed molecules or ions into surroundings is called desorption. Adsorption can be divided into physical adsorption and chemical adsorption depending on an absence or presence of electron transfer between adsorbed molecule (adsorbate) and adsorbent surface. Physical adsorption occurs due to weak attractive force such as van der Waals force. On the other hand, chemical adsorption is an adsorption is caused by the chemical bond formation between adsorbate and adsorbent with the electron transfer. Even before activated carbons were artificially designed and manufactured, human beings have empirically recognized the adsorptive performance of charcoal and used it as an adsorbent for removing odor, color and impurities. And nowadays, we manufacturing various shaped activated carbons such as crushed, powdered, pelletized, spherical, and fiber types [2]. Also we can produce activated carbon from various raw materials such as palm shell, husk, wood, coal, petroleum, polymer, and so on [3-6].

Due to the well-developed pore structure and its surface functionality, activated carbon is widely used in various fields as adsorbent and catalyst support. For example, activated carbon is used for water purification [7-9] and air purification [10, 11]. The US Departments of Energy (DOE) are looking for ways to using the high chemical energy of hydrogen (39 kWh/kg). Since hydrogen gas has a risk of explosion, the safe storage and transportation method are required. As a solution to this problem, research on hydrogen adsorption methods using porous materials such as activated carbon is proceeding [12, 13]. In addition, to its application to water treatment and exhaust gas refining, activated carbon in recent years is becoming more and more demanding as a functional carbon material. On the other hand, the catalyst carrier is a high specific surface area material used for highly dispersing the catalyst. The catalyst has a problem that the number of active sites decreases due to sintering and aggregation during the process. Decreasing the number of active sites not only reduces the overall reactivity, but can also induces catalytic degradations, giving rise to a reduction of the quality of the product. To prevent catalytic degradation, activated carbon with a high specific surface area is used as a support to disperse the catalyst particles and maintain the performance [14-16].

In addition, activated carbon with a high specific surface area is also required for energy storage devices such as electric double-layer capacitors (EDLCs) and Li-S batteries. Li-S batteries have a Li metal // sulfur type cell structure and are charged and discharged by the electrochemical reversible reaction of lithium and sulfur compounds [17, 18]. In Li-S battery, sulfur should be supported to porous material to form an electrode. To supporting sulfur, activated carbon is known to be the most suitable material, because of the excellent sulfur adsorption amount per electrode weight, electric conductivity, inexpensive price, and chemical stability. Also, EDLC, one of the ultra-high capacity supercapacitors, has the form of activated carbon // activated carbon symmetric electrode type [19-21]. EDLC has high output

performance by utilizing the principle of storing / releasing energy based on the principle that electrolyte ions form an electric double layer on the anode and cathode. When an external power supply is applied, anions and cations are attracted to the positive and cathode electrodes, respectively. During discharge, the stored energy is released by the diffusion of ions into electrolyte. Therefore, the specific surface area should be secured so that ions can be adsorbed as much as possible. EDLC electrodes using activated carbon are often used because of their excellent output density per weight (W/kg) and low price.

In order to further improved the performance of devices, it is required to increase of the degree of pore development of activated carbon, control the pore structure, and innovate of the activated carbon manufacturing method.

1.2 Manufacturing of activated carbon

Generally, activated carbon is manufactured by activation process. Activation process of carbon material is mainly classified by physical and chemical activation method. Physical activation reaction of carbon material is based on gasification of solid carbon atoms consisting of the carbon materials [22, 23]. The pore structure is developed by the controlled partial gasification reaction at the specific reaction site. As an agent that can cause the gasification reaction, an appropriate reactivity with the solid carbon atoms is required. For example, nitrogen, methane and carbon monoxide have relatively weak reactivity and they are not suitable as activation agents. On the other hand, oxygen has extremely high reactivity with carbon at high temperatures. Also, activation by oxygen is an exothermic reaction, so it is impossible to control. In contrast, carbon dioxide (CO_2) and steam (H_2O) possess suitable properties as the activation agents in physical activation of carbon materials.

The gasification reaction by CO_2 is shown in the following equation.

$$C + CO_2 = 2CO \quad -40.8 \text{ kcal}$$

In addition, the gasification reaction by H_2O is shown in the following equation.

$$C + H_2O = H_2 + CO \quad -29.4 \text{ kcal}$$

$$C + 2H_2O = 2H_2 + CO_2 \quad -19.0 \text{ kcal}$$

Because of the endothermic reaction between carbon and CO_2 or H_2O, the control of gasification degree is easy. The advantage of the physical activation method is that the price of the activation agent is inexpensive, and obtained activated carbon can be used immediately without a post-treatment process. However, since this physical activation takes place for carbon atoms where the oxidizing gas can access, local gasification at outer surface often occurs,

giving rise to the lowering of the yield and the pore development degree. Therefore, activated carbon by physical activation is a mainly used to manufacture cheap activated carbon although its pore structure development is low.

The main reaction of chemical activation is catalytic gasification by metal ions and hydroxide ions of the oxidizing agent. The most representative chemical activation mechanism by potassium hydroxide is shown in the following equations [24, 25].

$$2KOH \rightarrow H_2O + K_2O$$

$$C + H_2O \rightarrow H_2 + CO$$

$$CO + H_2O \rightarrow CO_2 + H_2$$

$$K_2O + CO_2 \rightarrow K_2CO_3$$

$$K_2O + H_2 \rightarrow 2K + H_2O$$

$$C + K_2O \rightarrow 2K + CO$$

When KOH, NaOH, $ZnCl_2$, or others is used as an activation agent, a neutralization/washing process using an acidic solution as post-treatment is necessary to remove intermediate strong base products in entire reaction. In addition, the high price of the activating agent for chemical activation compared to that for physical activation also affects the production cost of chemically activated carbon. However, activated carbon by chemical activation has an overwhelmingly high pore development degree, so it can be used such as hydrogen or energy storage device that requires high adsorption performance.

New methods such as the microwave method, the two-step activation method, and the nano-metal catalyst method have been proposed to produce activated carbon having higher pore

development degree [26-28]. However, as can be seen from the results of these studies, in order to obtain activated carbon with high yield and pore development degree, chemical activation is required consequently. Thus, the manufacturing cost of activated carbon by microwave, two-step activation, and nano-metal catalyst method is much higher than the existing physical and chemical activation. Therefore, there is a need for a new and facile manufacturing method for activated carbon having a high yield and a high pore structure with low manufacturing cost.

1.3 Interpretation of the pore structure on activated carbon by microdomain model

In order to make activated carbon with high yield and high pore development, it is necessary to efficiently develop a pore structure on carbon material. And to develop efficient pore structure, it is necessary to understand the pore structure development more accurately. Regarding the traditional pore model (hole-, slit- shaped), Franklin *et al.* [29] described that the pore structure is the defect of carbon stack structure or crystallite (**Figure 1-1**).

In 1992, as shown in **Figure 1-2**, Kaneko *et al.* [30] calculated specific surface area by microcrystalline graphitic structures of microporous carbon fibers. And they described the interstices between micro-graphitic walls may be classified into open and partially closed pores and an interstitial cage surrounded with neighboring micro-graphite. Furthermore, the open and partially closed pores are classified into slit and wedge-shaped micropores. Ruike *et al.* [31] reported microporous structure on carbon in 1994. Ruike model is shown in **Figure 1-3**. Their model was based on the Kaneko model, however, they explained about micropore and closed pore additionally. As a result of analyzing the carbon aerogel by the Monte-Carlo simulation method, Gavalda *et al.* [32] found that aerogel spheres with a 6 nm diameter to form a carbon aerogel, and 3 to 15 nm of mesopores and 0.7 to 1.5 nm of micropores (**Figure 1-4**). In addition, as a result of observation using a scanning tunneling microscope, Pfeifer *et al.* [33] reported the pore structures having shape of channels. At this moment, the depth of the pores by the channel was from 2.8 to 3.0 nm, and the channel width was from 1.5 to 2.0 nm.

However, these models cannot exactly explain about pore structure so far, and a new structural model is required for more accurate pore structure analysis. Unlike the suggestions of these structural models, our research group have presented a pore development model based on the microdomain structure. Our research group have been found finer units under particle level in

1995 [34]. After that, our research group suggested domain and microdomain structure is exist in carbon fiber [35]. Based on the domain and microdomain structure, our research group proposed a hierarchical carbon structure model [36]. Furthermore, our research group suggested that pore structure development can be explained by microdomain structure model. Our research group reported the development of slit-shaped micropores intra-microdomain and cylindrical mesopores are on inter-microdomains [37]. From our previous researches, I would like to suggest that it can be possible to selectively develop a unique pore structure for the purpose by understanding of the pore structure based on such a microdomain structure.

In a previous study, our research group have found that carbon particles are considered to be aggregates of a large number of basic structural units called microdomains [36]. Based on this microdomain structure model of carbon materials, a new model of pore structure of activated carbons has been proposed as a result of observing physically activated carbon fibers using scanning electron microscope and scanning tunnel-electron microscope [37]. In addition, as a result of observing activated carbon fibers prepared from the same raw material but different degrees of activation, it has been reported that the microdomain diameter distribution and the average microdomain size tended to decrease as the pore structure developed [37]. Furthermore, as a result of investigations of activated carbons prepared by physical and chemical activation methods from the same raw material, it has been found that the chemical activation method did not change the diameters of the particles and microdomains even if the degree of pore development increased [48]. In the case of the chemical activation, pore development progressed homogeneously overall for all microdomains consisting of carbon particles without apparent morphological change. However, the physical activation caused inhomogeneous gasification from the outer surface of the particle and microdomain due to the lower diffusibility of activation agent, giving rise to lower pore development and activation

yield. Therefore, if the inhomogeneous gasification can be improved, it would be possible to produce activated carbon with high activation yield and high specific surface area by cheap physical activation method.

1.4 Objective of this study

Based on various analysis and manufacturing methods, in numerous research groups related on activated carbon, methods to develop pores more effectively while increasing the understanding of the pore structure have been studied. Until now, however, the activated carbon by the physical activation method has a specific surface area of about 2000 m^2/g and an average pore diameter of 1.2 nm. These porosity of physical activation is reached almost the upper limit, and no process for producing advanced activated carbon by the physical activation method has been developed. Even if the specific surface area of 2000 m^2/g is achieved by the physical activation method, the yield is extremely low. By the chemical activation, on the other hand, it is possible to produce activated carbon with high yield and high degree of pore structure development, but the production cost of activated carbon is about dozen times higher.

The purpose of this study is to propose a method that can produce activated carbon with high yield and high activation degree at low cost, as opposed to the existing physical activation method. After showing the new possibilities, it was aimed at a development of a production process of activated carbon with a low-cost, high-yield and high-development pore structure. Furthermore, applicability of activated carbons produced by the developed new method to advanced devices was also examined.

This thesis consists of 6 chapters as follows.

In Chapter 1, I would like to introduce about activated carbon and its pore structure, manufacturing activated carbon and interpretation of the pore structure on activated carbon by microdomain model. Also, the objective of the study was mentioned.

In Chapter 2, I described evaluation methodologies of activated carbon. The gas adsorption method, which is the most widely used for the analysis of the pore structure of activated carbon, and the specific surface area calculation method and density functional theory based on the gas adsorption method were introduced. In addition, scanning electron microscope and scanning tunnel-electron microscope was introduced as an observation method to evaluate activated carbon. Furthermore, ^{129}Xe nuclear magnetic resonance was also introduced, which is being discussed as a new method for analyzing the pore development degree and pore shape of activated carbon. Additionally, density measurement of activated carbon was described.

In Chapter 3, I would like to establish a method for high yield and pore development degree of activated carbon by the pressurization. Firstly, we attempted to elucidate the effect of pressurization on the activated carbon yield, pore development degree and other factors. It was confirmed that the gasification, the main reaction of physical activation, was promoted by pressurization. Next, in order to investigate the effect of pressurization on particles, microdomain, and pore structure, activated carbon sample was prepared using magnetic suspension balance - thermogravimetry and the pore development degree was evaluated. As a result, it was confirmed that when compared with the atmospheric physical activation condition, the specific surface area is significantly increased by pressurized physical activation. In addition, many large micropores were introduced by pressurization from the pore size distribution results. As a result of microdomain observation, it was confirmed that the cause of the difference in the high specific surface area and the pore size distribution was due to the difference in the size and development of the microdomains between atmospheric and pressurized physical activation. However, since the morphology and particle size distribution of the activated carbon do not change significantly by pressurization, it means that the heterogeneous gasification reaction on the outer surface of the particles has been improved.

Consequently, it was possible to confirm the effect and possibility of the pressurized physical activation method onto particle and microdomain.

In Chapter 4, I suggested “Pressurized physical activation” method as a facile manufacturing method of activated carbon having high yield and pore development degree. Physical activation methods are commonly adopted in industry because of their low production costs, but the lack of activating agent diffusibility into core parts of the particles and microdomains of carbon materials causes a lower activation yield and degree of pore development, compared with chemical activation methods. To increase the diffusibility of activating agent into carbon material and corresponding degree of pore development, I propose a novel pressurized physical activation method. Pressurization showed remarkable increases in specific surface area and total pore volume of the prepared activated carbon, compared with atmospheric physical activation. Additionally, in activated carbon prepared by pressurization, pore size distribution analysis revealed characteristic development of micropores of about 1.6 nm; such micropores did not appear in activated carbon under conventional atmospheric physical activation. Furthermore, observations of particles and microdomains showed that pressurization increased the diffusibility of activation agent in carbon particles, but not at the microdomain level. This innovative pressurized physical activation can produce activated carbon with highly developed pores (specific surface area > 2,600 m^2/g) and a unique pore size distribution due to the improved activating agent diffusibility in carbon particle level.

In Chapter 5, I applied pressurized activated carbon as adsorbent for ethanol adsorption heat pump. Although chemically activated carbon with highly developed pore structures exhibits good ethanol adsorption performance, high activated carbon manufacturing costs inhibit its practical application as an adsorption heat pump adsorbent. Moreover, although physical activation can produce inexpensive activated carbon, the limited pore development limits the

ethanol adsorption performance. Recently, we developed a pressurized physical activation method that can produce activated carbon with a well-developed pore structure and characteristic pore size distribution with relatively high yield. In this study, we investigated the applicability of the pressurized physically activated carbon as an adsorbent in activated carbon–ethanol type adsorption heat pump system. Because of the large proportions of appropriate size pores by pressurization, the pressurized physically activated carbon showed effective ethanol adsorption performance comparable with that of chemically activated carbon on a weight basis. Furthermore, on a volume basis, the pressurized physically activated carbon, with a high bulk density, showed much higher effective ethanol adsorption performance than chemically activated carbon. These results reveal the potential of the pressurized physically activated carbon as a relatively inexpensive high-performance adsorbent for adsorption heat pump systems with ethanol refrigerant.

In Chapter 6, obtained results and discussions in this thesis were summarized as conclusion.

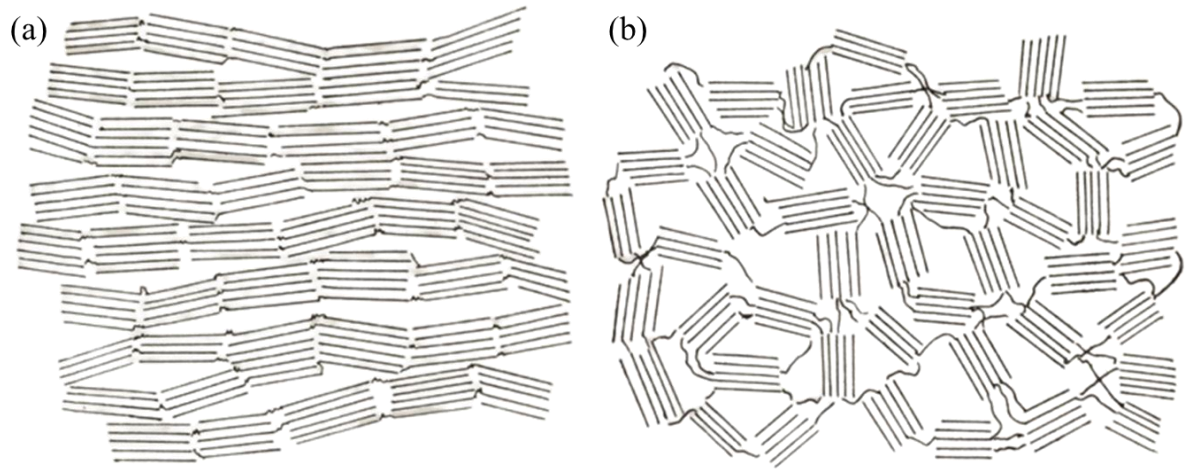

Figure 1-1. Franklin model of (a) graphitizable carbon and (b) non-graphitizable carbon [29].

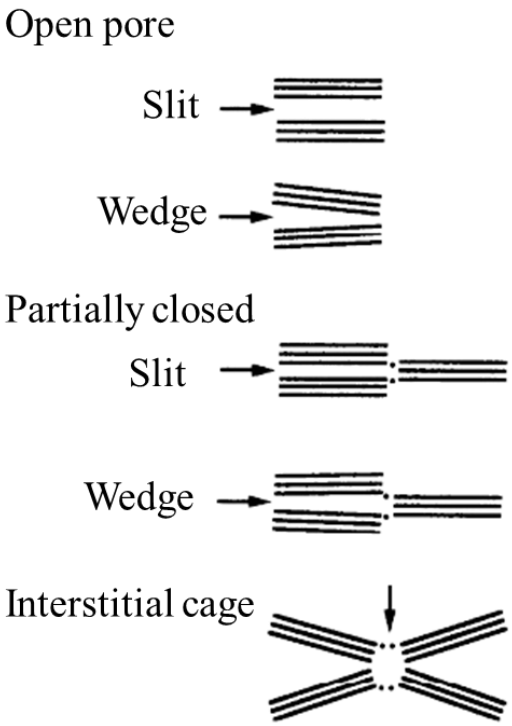

Figure 1-2. Schematic image of open, partially closed and interstitial cage shape pore by Kaneko model [30]. ("Reprinted from Journal of Carbon, 30, 5211751437883, K. Kaneko, *et al.*, Origin of superhigh surface area and microcrystalline graphitic structures of activated carbons, 1075-1088, 1992, with permission from Elsevier").

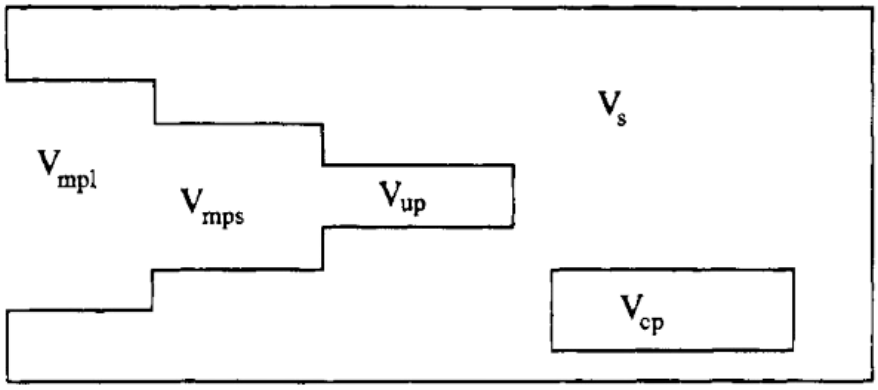

Figure 1-3. Pore structure model on activated carbon by Ruike [31]; V_s: volume of carbon substrate, V_{mpl}: large micropore volume, V_{mps}: small micropore volume, V_{up}: ultra-micropore volume, V_{cp}: closed pore, respectively. ("Reprinted (adapted) with permission from M. Ruike, *et al.*, Inaccessible pore characterization of less-crystalline microporous solids, *J. Phys. Chem.*, **98**, (1994) 9594–9600. Copyright 1994 American Chemical Society").

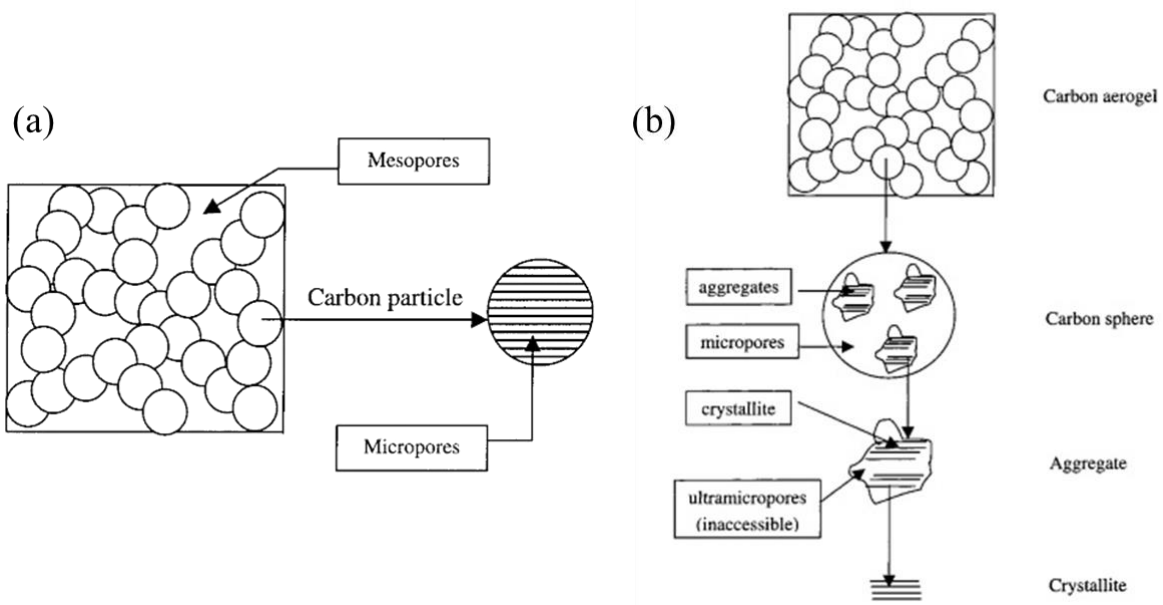

Figure 1-4. (a) Mesopores and micropores in carbon aerogel. (b) Hierarchical pore structures in carbon aerogel modeling by Gavalda [32]. ("Reprinted (adapted) with permission from S. Gavalda, *et al.*, Nitrogen Adsorption in Carbon Aerogels: A Molecular Simulation Study, *Langmuir*, **18**, (2002) 2141–2151. Copyright 2002 American Chemical Society").

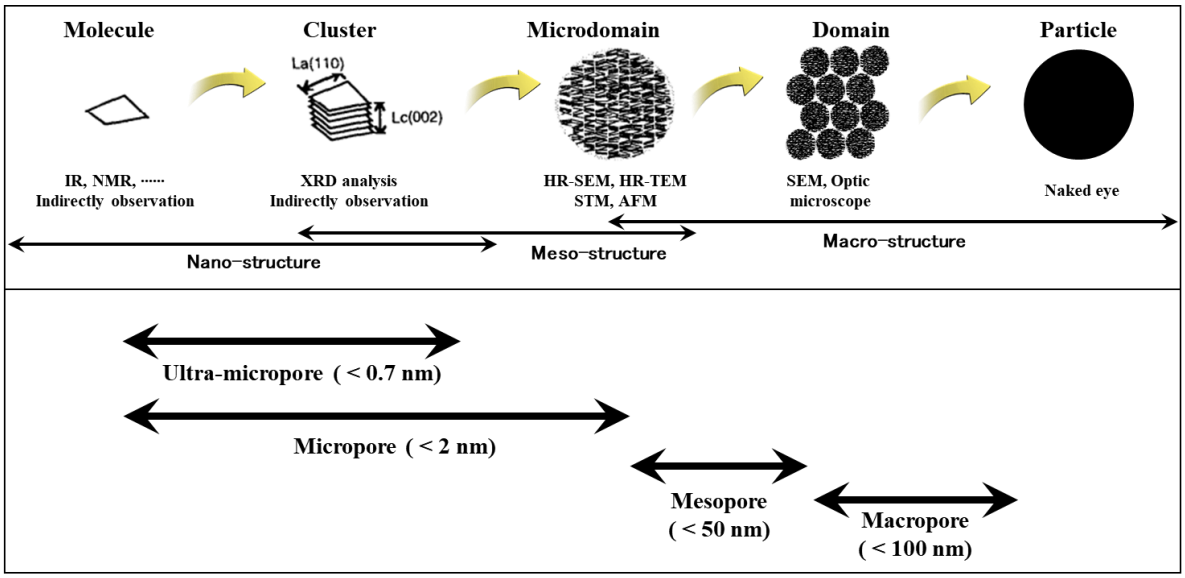

Figure 1-5. Comparison of hierarchical structure model of carbon material based on microdomain structure [36] and pore size classification by IUPAC.

References

[1] J. L. Figueiredo, M. F. R. Pereira, M. M. A. Freitas, J. J. M. Orfao, Modification of the surface chemistry of activated carbons, *Carbon*, **37** (1999) 1379–1389.

[2] H. Marsh, F. Rodriguez-Reinoso, Activated carbon, 1st edition, Elsevier science, (2006).

[3] O.S. Amuda, A.A. Giwa, I.A. Bello, Removal of heavy metal from industrial wastewater using modified activated coconut shell carbon, *Biochemical Engineering Journal*, **36** (2007) 174–181.

[4] T Zhang, W. P. Walawendera, L.T. Fana, M Fan, D. Daugaard, R.C. Brown, Preparation of activated carbon from forest and agricultural residues through CO2 activation, *Chemical Engineering Journal*, **105** (2004) 53–59.

[5] A. M. Cunliffe, P, T. Williams, Influence of process conditions on the rate of activation of chars derived from pyrolysis of used tires, *Energy & Fuels*, **13** (1999) 166–175.

[6] E. Raymundo-Pinero, D. Cazorla-Amoros, A. Linares-Solano, J. Find, U. Wild, R. Schlogl, Structural characterization of N-containing activated carbon fibers prepared from a low softening point petroleum pitch and a melamine resin, *Carbon*, **40** (2002) 597–608.

[7] K. Kadirvelu, M. Kavipriya, C. Karthika, M. Radhika, N. Vennilamani, S. Pattabhi, Utilization of various agricultural wastes for activated carbon preparation and application for the removal of dyes and metal ions from aqueous solutions *Bioresource Technology*, **87** (2003) 129–132.

[8] D. Mohana, Charles U. Pittman Jr. Arsenic removal from water/wastewater using adsorbents—A critical review*, Journal of Hazardous Materials*, **142** (2007) 1–53.

[9] Md. Ahmaruzzaman, Adsorption of phenolic compounds on low-cost adsorbents: A review *Advances in Colloid and Interface Science*, **143** (2008) 48–67.

[10] W. Feng, S. Kwon, E. Borguet, R. Vidic, Adsorption of hydrogen sulfide onto activated

carbon fibers: Effect of pore structure and surface chemistry, *Environ. Sci. Technol.*, **39** (2005) 9744–9749.

[11] P. Lua, C. Li, G. Zenga, L. He, D. Penga, H. Cui, S. Li, Y. Zhai, Low temperature selective catalytic reduction of NO by activated carbon fiber loading lanthanum oxide and ceria *Applied Catalysis B: Environmental,* **96** (2010) 157–161.

[12] L. Schlapbach, A. Züttel, Hydrogen-storage materials for mobile applications *NATURE*, **414**, 15 (2001) 353–358.

[13] H. Furukawa, O. M. Yaghi, Storage of hydrogen, methane, and carbon dioxide in highly porous covalent organic frameworks for clean energy applications, *J. AM. CHEM. SOC.*, **131** (2009) 8875–8883.

[14] F. Rodriguez-Reinoso, The role of carbon materials in heterogeneous catalysis, *Carbon*, **736**, 3 (1998) 159–175.

[15] Z. Liu, X.Y. Ling, X. Su, J. Y. Lee, Carbon-supported Pt and PtRu nanoparticles as catalysts for a direct methanol fuel cell *J. Phys. Chem. B*, **108** (2004) 8234–8240.

[16] E. Auer, A. Freund, J. Pietsch, T. Tacke, Carbons as supports for industrial precious metal catalysts *Applied Catalysis A: General*, **173** (1998) 259–271.

[17] J. Wang, S. Kaskel, KOH activation of carbon-based materials for energy storage *J. Mater. Chem.*, **22** (2012) 23710–23725.

[18] P. G. Bruce, S. A. Freunberger, L. J. Hardwick, J.Tarascon, Li–O2 and Li–S batteries with high energy storage, *Nature materials*, **11** (2012) 19–29.

[19] Elzbieta Frackowiak, Francois Beguin Carbon materials for the electrochemical storage of energy in capacitors *Carbon*, **39** (2001) 937–950.

[20] P. Simon, Y. Gogotsi, Materials for electrochemical capacitors, *Nature materials*, **7** (2008)

845–854.

[21] Y. Zhai, Y.Dou , D. Zhao, P. F. Fulvio , R. T. Mayes, S. Dai, Carbon materials for chemical capacitive energy storage, *Adv. Mater.*, **23** (2011) 4828–4850.

[22] M. Molina-sabio, M. T. Gonzalez, F. Rodriguez-Reinoso, A. Sephijlveda-Escribano, Effect of steam and carbon dioxide activation in the micropore size distribution of activated carbon, *Carbon* **33**, 1 (1995) 15–23.

[23] F. Rodriguez-Reinoso, M. Molina-sabio, M. T. Gonzalez, The use of steam and CO2 as activation agents in the preparation of activated carbons, *Carbon,* **34**, 4 (1996) 505–509.

[24] T. Otowa, Y. Nojima, T. Miyazaki, Development of KOH activation high surface area carbon and its application to drinking water purification, *Carbon,* **35**, 9 (1997) 1315–1319.

[25] T. Otowa, R. Tanibata, M. ltoh, Production and adsorption characteristics of MAXSORB: high-surface-area active carbon, *Gas Separation & Purification* **7**, 4 (1993) 241–245.

[26] E. Yagmur, M. Ozmak, Z. Aktas, A novel method for production of activated carbon from waste tea by chemical activation with microwave energy, Fuel, **87** (2008) 3278–3285.

[27] A.H. Basta, V. Fierro, H. El-Saied, A. Celzard, 2-Steps KOH activation of rice straw: an efficient method for preparing high-performance activated carbons, *Bioresour. Technol.* **100**, 17 (2009) 3941–3947.

[28] J. Xue, L. Huang, F. Jin, Q. Liu, G. Liu, M. Wang, et al., Two novel and simple strategies for improvement of the traditional activation method for activated carbon preparation: nano-copper catalysis and Cu(II) doping, *RSC Adv.* **5** (2015) 81857–81865.

[29] R. E. Franklin, Crystallite growth in graphitizing and non-graphitizing carbons, *Proceedings of the Royal Society of London A: Mathematical, Physical and Engineering Sciences. The Royal Society*, **209** (1951) 196–218.

[30] K. Kaneko, C. Ishii, M. Ruike, H. Kuwabara, Origin of superhigh surface area and

microcrystalline graphitic structure of activated carbons, *Carbon*, **30** (1992) 1075–1088.

[31] M. Ruike, T, Kasu, N. Setoyama, T. Suzuki, K. Kaneko, Inaccessible pore characterization of less-crystalline microporous solids, *J. phys. chem.*, **98** (1994) 9594–9600.

[32] S. Gavalda, K. E. Gubbins, Y. Hanzawa, K. Kaneko, K. T. Thomson, Nitrogen adsorption in carbon aerogels: A molecular simulation study, *Langmuir*, **18** (2002) 2141–2151.

[33] P. Pfeifer, F. Ehrburger-Dolle, T. P. Rieker, M. T. González, W. P. Hoffman, M. Molina-Sabio, F. Rodríguez-Reinoso,5 P. W. Schmidt, D. J. Voss, Nearly space-filling fractal networls of carbon nanopores, *Phys. Rev. Lett.*, **88** (2002) 115502.

[34] S. -H. Yoon, Y. korai, I. Mochida, K. Yokogawa, S. Fukuyama, M. Yoshimura, Axial nano-scale microstructures in graphitized fiber inherited from liquid crystal mesophase pitch, *Carbon*, **34** (1996) 83–88.

[35] I. Mochida, S.-H. Yoon, N. Takano, F. Fortin, Y. Korai, K. Yokogawa, Microstructure of mesophase pitch-based carbon fiber and its control, *Carbon*, **34** (1996) 941–956.

[36] I. Mochida, S. -H. Yoon, S. -Y. Lim, S. -H. Hong, Progress and effectiveness of structural models of carbons, *Tanso*, **215** (2004) 274–284.

[37] N. Shiratori, K. J. Lee, J. Miyawaki, S. -H. Hong, I. Mochida, B. An, K. Yokogawa, J. Jang, S. -H. Yoon, Pore structure analysis of activated carbon fiber by microdomain-based model. *Langmuir*, **25** (2009) 7631–7637.

[38] D.-W. Kim, H.-S. Kil, K. Nakabayashi, S.-H. Yoon, J. Miyawaki, Structural elucidation of physical and chemical activation mechanisms based on the microdomain structure model, *Carbon*, **114** (2017) 98–105.

Chapter 2.

Methodology

2.1 Pore structural analysis

Gas adsorption method is established to characterize pore structures [1]. There are two types of gas adsorption isotherm measurement methods; the gravimetric method and the volumetric method. In the gravimetric method, adsorption amount is directly obtained by measuring the weight change of an adsorbent at different gas pressures using weighing equipment such as a quartz spring, an electronic balance, etc. The volumetric method is a method of calculating the amount of adsorption from the pressure change using the combined gas law. For both methods, temperature of sample is well-controlled using cryogen, water/oil bath, heater, and so on, though, in the case of the volumetric method, manifold temperature is also needed to be kept constant. The gases used in gas adsorption methods mainly include nitrogen, argon, carbon dioxide, xenon, water vapor, and so on [2].

In 1985, IUPAC issued “Reporting Physisorption Data for Gas / Solid Systems” regarding pore structure classification, measurement and calculation of surface area / porosity. Pore structure classification by IUPAC in 1985 is shown in **Figure 2-1**. The report by IUPAC is widely accepted by the scientific and industrial fields [3]. However, over the past decades, various new characteristic types of isotherms have been identified and shown to be closely related to pore structure and its shape. Therefore, in 2015, IUPAC reported newly classifications of physical adsorption isotherms. The updated classification of physical adsorption isotherms is shown in **Figure 2-2** [4]. Type I is an isotherm curve commonly found in chemical adsorption or microporous materials such as activated carbon. Of them, Type I(a)

appears when narrow pores (1 nm or less) are present, and type I(b) is observed when a wide range of micropores and narrow mesopores exist. Types II and III are found in non-porous or macro-porous materials. The interaction between the adsorbent and the adsorbed molecule (adsorbate) is weaker in Type III than in Type II. Type IV is mainly found for the adsorbent with mesopores. In Type IV(a), a hysteresis loop generated by the capillary condensation is observed. On the other hand, Type IV(b) isotherms are also provided by conical and cylindrical mesopores that are closed at the tapered ends. Type V is similar to Type IV, but is seen when the interaction between the solid and the adsorbed molecule is weak. Type VI isotherms represent a layer-by-layer adsorption on a very uniform non-porous surface. For nitrogen and argon adsorptions at 77 K and 87 K, respectively, Type I(a) isotherms are given by microporous materials having mainly narrow micropores (< 1 nm size); Type I(b) isotherms are found with materials having pore size distributions over a broader range including wider micropores and possibly narrow mesopores (< 2.5 nm size).

Various calculative analysis methods have been proposed to obtain pore structural parameters such as specific surface area and pore volume from the adsorption isotherm curves obtained by the abovementioned gas adsorption methods. The BET method which has been proposed by S. Brunauer *et. al.* is a well-known analysis method based on the multi-layer physical adsorption process on a flat surface [5]. In the BET analysis, the specific surface area is commonly calculated using the adsorption amount in the range of relative pressure P/P_0 = 0.05 to 0.3. Here, in the case of adsorption on the flat surface, the relative pressure P/P_0 = 0.05 is the pressure at which the adsorption of the monolayer is almost completed, and at the relative pressure P/P_0 = 0.35, the molecule is in the process of adsorbing to the second layer as reported by the simulation study [5]. By the BET analysis, the adsorption amount of the monolayer can be obtained by using the adsorption amount when the adsorption of the second layer proceeds

after the adsorption of the first layer is completed. However, for porous materials whose pore diameter is 2 nm or less, that is, microporous materials, the adsorbed molecules receive the interactions from opposed pore walls, but not from one-side surface. Therefore, the unexpected adsorption is promoted in micropores. The actual adsorption amount is larger than the ideal adsorption amount of the BET model, and the analysis result often gives a overestimated specific surface area than the actual value. For this reason, the BET analysis should not be applied to microporous materials with a pore diameter of 2 nm or less like activated carbon.

Although many methods for analyzing 77 K nitrogen or 87 K argon adsorption isotherms other than the BET method have been proposed, analysis by the α_S-plot method [6–8] is considered to be desirable for porous materials. The α_S-plot is a method for analyzing unknown samples by comparing the adsorption isotherms of standard samples and unknown samples. In the α_S-plot analysis, the nitrogen adsorption isotherm of the standard sample is converted so that it becomes a straight line, and information on the unknown sample can be obtained by comparing the standard sample with the unknown sample. From this analysis, the values of the total specific surface area, the external specific surface area, and the total pore capacity can be obtained. The average pore width can be calculated by assuming the pore shape using the obtained values of specific surface areas and pore volume. For example, assuming a slit type pore, if the total specific surface area is S_{total}, the outer specific surface area is S_{ext}, and the micropore capacity is V, the average pore width w of the micropores is calculated by the following equation [9].

$$w = 2V \times 1000 / (S_{total} - S_{ext}) \text{ [nm]}$$

The average pore width w obtained by this equation shows a relatively good agreement with the values from other analysis methods.

Recently, the calculated absorption isotherms can be easily obtained based on the density functional theory (DFT) method [10–12] and the Grand Canonical Monte Carlo (GCMC) method [13], which have become possible due to the development of computers in recent years. By using the DFT and GCMC, important pore structure information such as pore size distribution, total pore volume, micro- and meso-pore volume can be obtained.

2.2 Observational analysis

Many studies have been conducted to understand the pore structure of activated carbon. In the previous studies, since direct observation was quite difficult, gas adsorption techniques or simulation methods by modeling have been mainly conducted. With the development of technology, however, it becomes possible to directly obtain information of the pore structure in these days.

Scanning electron microscope (SEM) images the electronic signals of secondary electrons and backscattered electrons emitted from the surface of a sample when the surface of the sample is irradiated with an electron beam. At low magnification, it is effective for observing particles of activated carbon, and at high magnification, micropores can also be observed in recent years. However, since only a local image on the particle surface is obtained by SEM, there is still a limitation for quantitative analysis of the entire pore structures.

Scanning tunneling microscope (STM) is an analytical method for observing the surface state by tunneling current [14]. When a bias voltage is applied between the very close to the sample surface and the probe that the micrometer-level thickness tip, electrons can pass through the potential barrier due to the tunnel effect. The result of tunneling current is determined by the distance of the probe and sample, the applied voltage, and the interaction with the sample. An image can be obtained by measuring the tunnel current flowing between the probe and the sample while scanning the sample surface. By using STM, the mean size of microdomains and the microdomain size distribution can be obtained.

2.3 Other methods

^{129}Xe-NMR method is a state-of-the-art technology that is drawing attention in pore structure analysis. From ^{129}Xe-NMR measurement results for adsorbed Xe gas on porous material, correlated graph has been obtained with the chemical shift value at the peak top on the horizontal axis and the average pore diameter on the vertical axis [15]. According to the results of this report, not only the degree of pore development but also information of pore shape can be estimated. It is thought that different pore structures such as cylindrical shape and slit-like shape would give different interaction strength between pore and adsorbate, and thus different correlations will be given for each pore type. Indeed, as shown in **Figure 2-3**, different correlation curves from that for the cylinder type pores were obtained for the slit type pores [15, 16]. Additionally, it has been confirmed that the correlation was independent from dominant components of porous materials: Both silica-based mesoporous materials and mesoporous carbons gave the same correlation curve. This result indicates that the correlation is mainly the pore shape dependent, suggesting a potential of ^{129}Xe -NMR technique as an analytical method of pore shape of porous materials.

Since activated carbon has a pore structure in carbon material, there is a correlation between the density of activated carbon and the degree of pore structure development. Density is divided into true density, bulk density, and apparent density. Because of the true density is a density of solid substance with the exception of any voids and pores, it is difficult to obtain for samples when micropores and/or closed pores are existing. Apparent density is the density of substance including closed pores but excluding open pores and voids. In a calculation of the bulk density, volumes include solid substance, closed pores, open pores, and voids between particles.

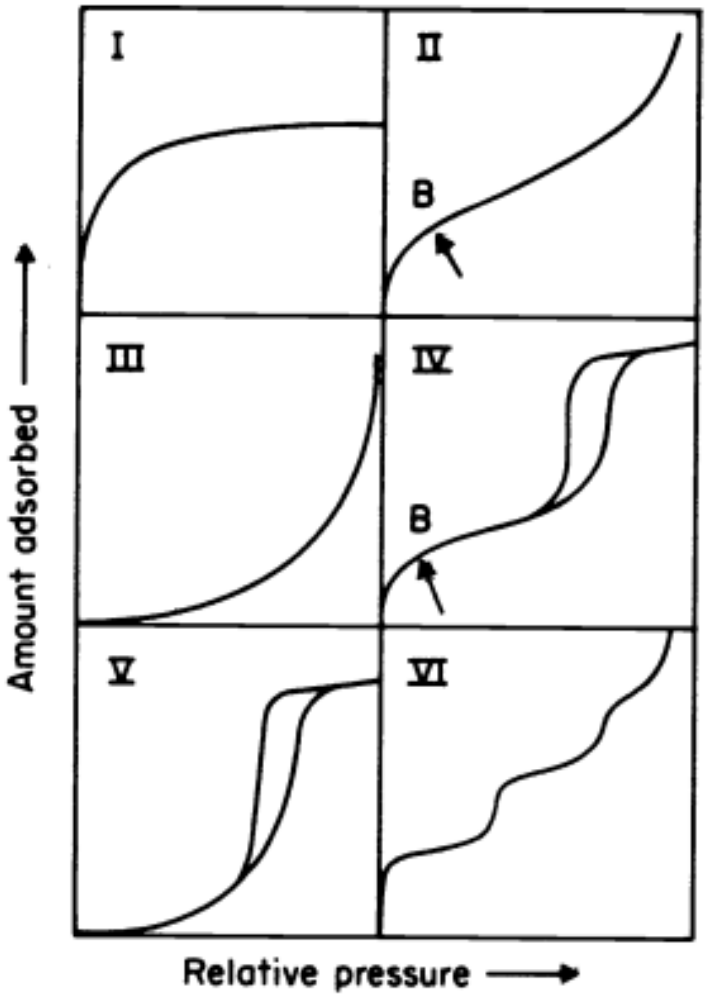

Figure 2-1. Classification of physical adsorption isotherm curves suggested by IUPAC in 1985 [3]. ("Reproduced with permission from K. S. W. Sing *et al.*, REPORTING PHYSISORPTION DATA FOR GAS/SOLID SYSTEMS with Special Reference to the Determination of Surface Area and Porosity, *Pure Appl. Chem.*, **57** (1985) 603–619. © IUPAC, Copyright 1985 De Gruyter").

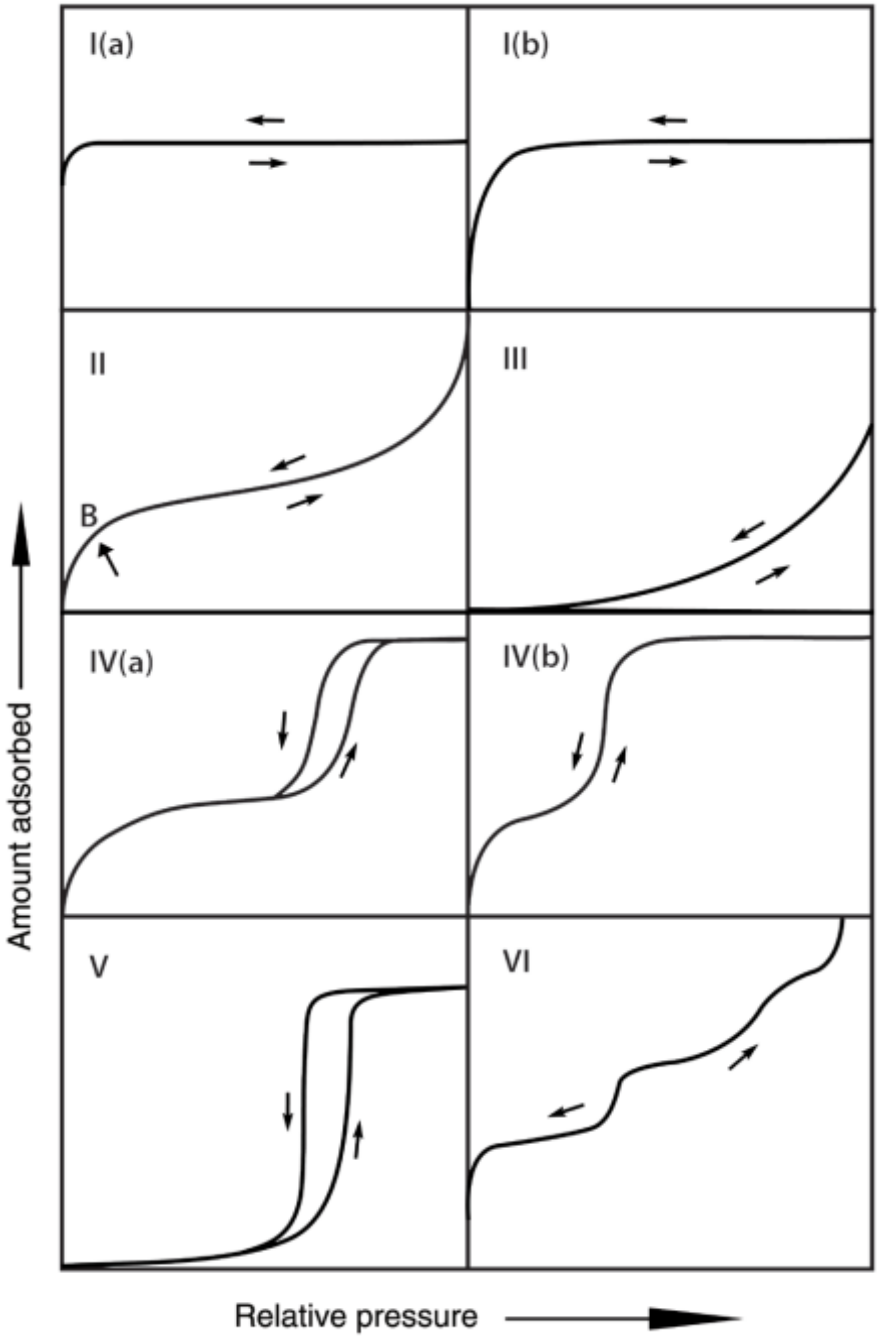

Figure 2-2. Classification of physical adsorption isotherm curves suggested by IUPAC in 2015 [4]. ("Reproduced with permission from M. Thommes *et al.*, Physisorption of gases, with special reference to the evaluation of surface area and pore size distribution (IUPAC Technical Report), *Pure Appl. Chem.*, **87** (2015) 1051–1069. © IUPAC, Copyright 2015 De Gruyter").

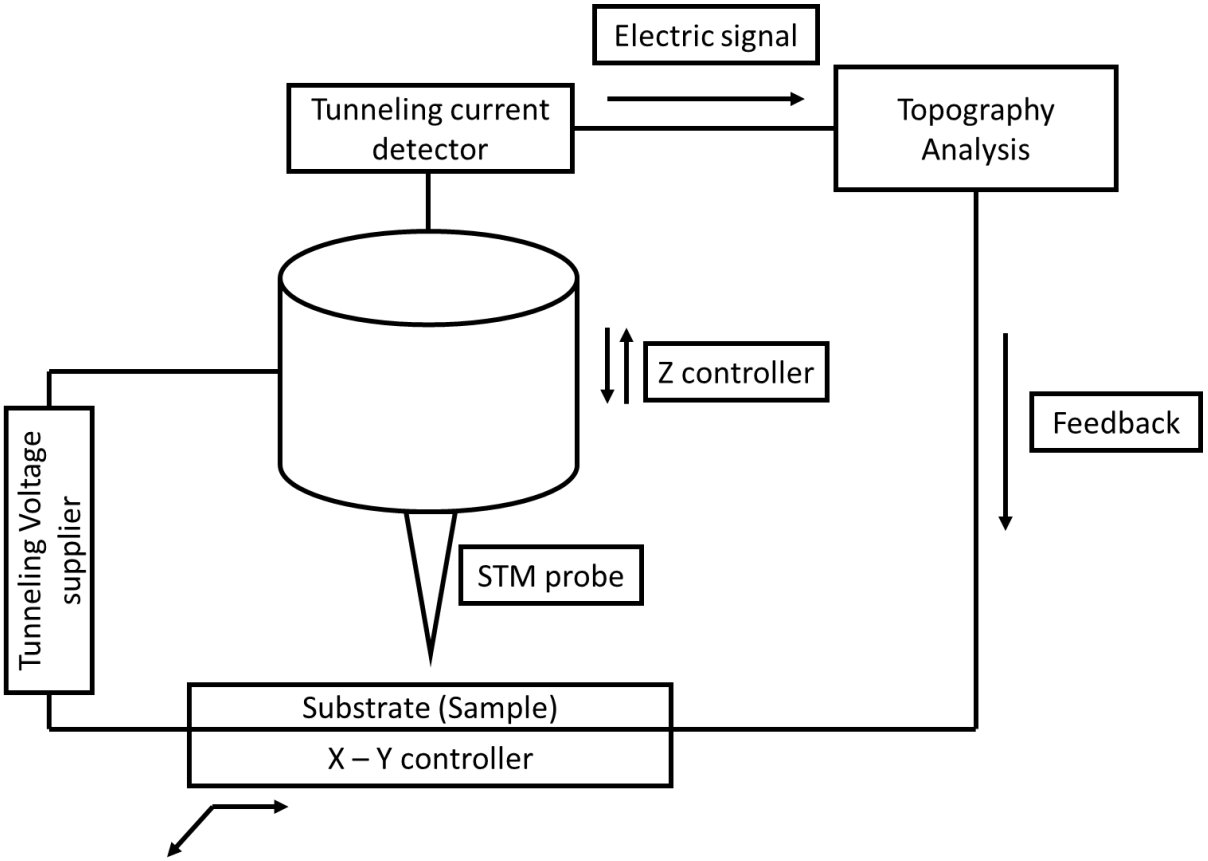

Figure 2-3. Schematic image of STM.

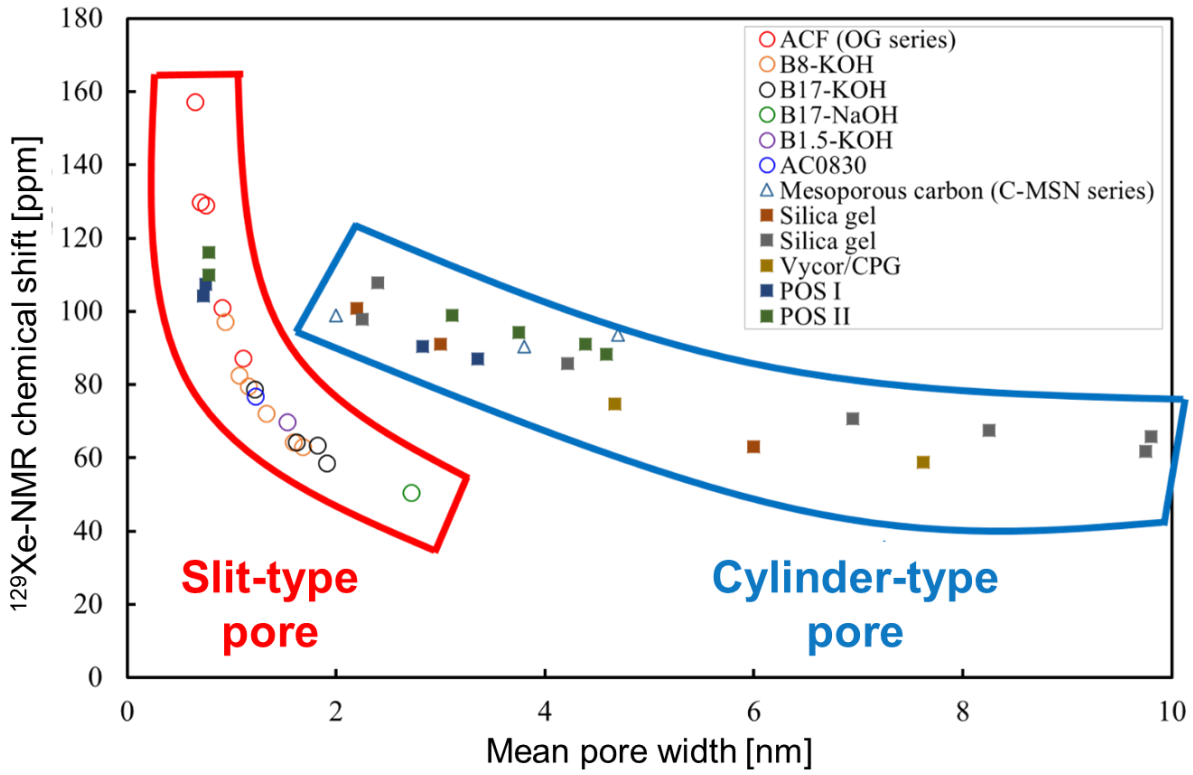

Figure 2-4. Difference in ^{129}Xe-NMR chemical shift and average pore size between slit type and cylinder type [15, 16].

References

[1] J. L. Figueiredo, M. F. R. Pereira, M. M. A. Freitas, J. J. M. Orfao, Modification of the surface chemistry of activated carbons, *Carbon*, **37** (1999) 1379–1389.

[2] D. Dollimore, P. Spooner, A. Turner, The BET method of analysis of gas adsorption data and its relevance to the calculation of surface areas, *Surface Technology*, **4** (1976) 121–160.

[3] K. S. W. Sing, D. H. Everett, R. A. W. Haul, L. Moscou, R. A. Poertti, J. Rouquerol, T. Siemieniewska, REPORTING PHYSISORPTION DATA FOR GAS/SOLID SYSTEMS with Special Reference to the Determination of Surface Area and Porosity, *Pure Appl. Chem.*, **57** (1985) 603–619.

[4] M. Thommes, K. Katsumi, A. V. Neimark, J. P. Oliver, F. Rodriguez-Reinoso, J. Rouquerol, K. S. W. Sing, Physisorption of gases, with special reference to the evaluation of surface area and pore size distribution (IUPAC Technical Report), *Pure Appl. Chem.*, **87** (2015) 1051–1069.

[5] S. Brunauer, P. H. Emmett, E. Teller, Adsorption of gases in Multimolecular layers, *J. Am. Chem. Soc.*, **60** (1938) 309–319.

[6] K. Kaneko, C. Ishii, M. Ruike, H. Kuwabara, Origin of superhigh surface area and microcrystalline graphitic structures of activated carbons, *Carbon*, **30** (1992) 1075–1088.

[7] C. P. Jaroniec, M. Kruk, and M. Jaroniec, A. Sayari, Tailoring surface and structural properties of MCM-41 silicas by bonding organosilanes, *J. Phys. Chem. B*, **102** (1998) 5503–5510.

[8] M. Jaroniec, M. Kruk, Standard nitrogen adsorption data for characterization of nanoporous silicas, *Langmuir*, **15** (1999) 5410–5413.

[9] K. Kaneko, Fundamentals of gas adsorption for characterization of carbon materials, *Tanso*, **186** (1999) 50–53

[10] P. I. Ravikovitch, A. Vishnyakov, R. Russo, A. V. Neimark, Unified approach to pore size characterization of microporous carbonaceous materials from N_2, Ar, and CO_2 adsorption isotherms, *Langmuir*, **16** (2000) 2311–2320.

[11] P. I. Ravikovitch, A. V. Neimark, Density functional theory of adsorption in spherical cavities and pore size characterization of templated nanoporous silicas with cubic and three-dimensional hexagonal structures, *Langmuir*, **18** (2002) 1550–1560.

[12] A. V. Neimark, Y. Lin, P. I. Ravikovitch, M. Thommes, Quenched solid density functional theory and pore size analysis of micro-mesoporous carbons, *Carbon*, **47** (2009) 1617–1628.

[13] B. Chen, J. J. Potoff, J. I. Siepmann, Monte Carlo calculations for alcohols and their mixtures with alkanes. Transferable potentials for phase equilibria. 5. United-atom description of primary, secondary, and tertiary alcohols, *J. Phys. Chem. B*, **105** (2001) 3093–3104.

[14] C. J. Chen, Introduction to scanning tunneling microscopy, *Oxford University Press*. (2008).

[15] V. V. Terskikh, I. L. Moudrakovski, S. R. Breeze, S. Lang, C. O. Ratcliffe, J. A. Ripmeester, A. Sayari, Characterization of porous glasses: Simulation models, adsorption isotherms, and the Brunauer-Emmett-Teller analysis method, *Langmuir*, **18** (2002) 5653–5656.

[16] K. Hata, H. -S. Kil, K. Ideta, K. Nakabayashi, I. Mochida, S. -H. Yoon, J. Miyawaki, Correlation between pore size of activated carbons and chemical shift of 129Xe-NMR, *Proceedings of The World Conference on Carbon (Carbon 2016),* P4–80.

Chapter 3.

Possibility of pressurized physical activation method

3.1 Introduction

As mentioned in Chapter 2, physical activation reaction is based on gasification of carbon material by oxidizing gas [1, 2]. Therefore, although it is possible to manufacture activated carbon at low cost, the yield and pore development of activated carbon are low [3, 4].

As explained in Section 1.3, the improvement of diffusibility of activating agent is considered to be a key to increase the degree of pore development and activation yield of physically activated carbon.

To increase diffusibility of activating agent into carbon material, pressurization is considered to be an effective way. Our research group have reported that the pressurization during the oxidative stabilization of isotropic and mesophase pitch fibers improved diffusivity of gas into core part of the fibers, allowing homogeneous stabilization at low temperature [8]. In addition, although not that much, it has been reported that the diffusibility of the oxidation gas into the carbon material was improved by pressurization [9–11]. From these studies, it was speculated that the diffusibility of the activating agent into the carbon material could be increased by pressurized during physical activation.

In this Chapter 3, a possibility of the pressurized physical activation as a preparation method of activated carbon of high activation degree was studied.

3.2 Experimental

3.2.1 Preliminary study to estimate activation conditions

As a raw material for activated carbon, an 8 μm spherical phenol resin (BEAPS series, ASAHI YUKIZAI CORPORATION, Japan) was applied to investigate the effects of pressurization on particle size and shape. At first, the resin was carbonized at 600℃ for 1 h in N_2 with a flow rate of 200 cm^3/min. The average carbonization yield was 52%. CO_2 was selected as the activating agent because of its easy handling. In this study, a magnetic suspension balance - thermogravimetry system (MSB-TG, **Figure 3-1**) was used for atmospheric and pressurized gasification. From the thermogravimetry curve, relationship between the activation conditions (temperature and pressure) and gasification rate was evaluated. The gasification rate was calculated as:

$$\text{Gasification rate [\%]} = \text{Gasified (decreased) weight [g]} / \text{Initial weight [g]} \times 100$$

3.2.2 Sample preparation

Based on the results in the preliminary examination in Section 3.2.1, activation conditions to obtain activated carbons with 18–20% yield were determined at each activation pressure of 0.1, 0.5, and 1.0 MPa. I designated the obtained activated carbon as PXTY, where X and Y indicate the activation pressure in MPa and stopped temperature in degree Celsius, respectively; for example, P0.1T920 indicates activated carbon prepared at 0.1 MPa and stopped at 920℃.

3.2.3 Characterization

To investigate pore characteristics, N_2 adsorption and desorption isotherms at 77 K were measured using a gas adsorption desorption analyzer (Nova-e series; Anton Paar QuantaTec Inc., USA). Pore structural parameters including total pore volume and specific surface area were calculated by the α_S-plot [13] and quenched solid density functional theory (QSDFT) [14] methods from the N_2 adsorption isotherms.

Particle size distribution and average particle size were investigated using a scanning electron microscope (SEM, JSM-6700F; JEOL, Japan), evaluating the mean size of 300 particles in SEM images of each sample. To investigate the microdomain size and structure, I also acquired scanning tunneling microscope (STM, Agilent Technologies 5500 Scanning Probe Microscope; Toyo Corporation, Japan) images, using its constant current mode (current: 0.3–1.2 nA, bias voltage: 0.1–1.5 V, and scan frequency: 1–2 Hz). Microdomain size distribution and mean size of microdomain were determined by 200 microdomains in STM images of each activated carbon sample.

3.3 Results and discussion

3.3.1 Preliminary study using MSB-TG

MSB-TG results are shown in **Figure 3-2**. At all pressures, a rapid weight loss (gasification) was observed from 700℃. It was considered that the gasification reaction with CO_2 started at around 700℃ on carbonized BEAPS. Furthermore, since the inflection point of the curve was observed at a lower temperature as the pressure increased, it can be seen that the temperature at which the gasification reaction started became lower by applying the pressure. This was the same tendency as reported in the previous study that the stabilization temperature decreasing occurred by pressurization on the stabilization process to the pitch-based carbon fiber [9]. For a direct comparison of gasification tendency, the temperatures required to achieve target gasification rates of 30, 50 and 70% under each pressure condition are shown in **Table 3-1**. At 0.1 MPa, each gasification rate was achieved at 895, 943 and 976℃. In contrast, at 0.5 MPa, it was achieved at 838, 886, and 924℃, respectively. Compared to 0.1 MPa, the temperature was about 50 to 60℃ lower at each gasification rate. It was also achieved at 762, 819 and 862℃ when pressurized to 1.0 MPa. It was confirmed that in the case of 1.0 MPa compared to 0.1 MPa, it is achieved at lower temperatures of about 90‐130℃. In 1.5 MPa, however, there are almost no change from 1.0 MPa. From these results, it was confirmed that the temperature for achieving a certain gasification rate decreased with an increase of the applying pressure. This result suggests that pressurization can accelerate and promote the gasification reaction.

3.3.2 Pore structure analysis results

N_2 adsorption isotherm results of the activated carbons prepared at different CO_2 pressure at

77 K are shown in **Figure 3-3**. Also, activation pressure, yield and pore structural parameters are shown in **Table 3-2**. All samples basically showed Type I adsorption isotherm curves, but P0.5T900 and P1T870 showed a slight hysteresis shape. As a result of the α_S-plot analysis, it was found that P0.1T920 had a specific surface area of about 1140 m^2/g and 0.6 cm^3/g of total pore volume. On the other hand, for P0.5T900, the N_2 adsorption amount clearly increased compared to P0.1T920, and a specific surface area of 1910 m^2/g and 1.2 cm^3/g of total pore volume was achieved. Furthermore, P1T870 showed further increased N_2 adsorption amount, and the specific surface area and total pore volume were 2680 m^2/g and 1.5 cm^3/g, respectively. These results revealed that the degree of pore structure development of pressurized physically activated carbon can exceed the limit of the conventional physically activated carbon. Changes of specific surface area and pore volume for each activated carbon prepared at different activation pressures are shown in **Figure 3-5**. By pressurization, specific surface area was increased proportionally. However, total pore volume increased a little bit compared to the specific area. This result suggests that P1T870 had wider pore size than others.

Pore size distribution was calculated by the QSDFT method from the 77 K nitrogen adsorption isotherm. As shown in **Figure 3-4**, it was confirmed that 0.6 to 2 nm micropores were introduced in P0.1T920. Especially, peak top was placed at 0.8 nm. On the other hand, it was found that the pores with a size of 1.2–3 nm were specifically increased in P0.5T900 as compared with P0.1T920. In addition, P1T870 showed a further development of pores of 1.2–3 nm. It was confirmed that the large amount of wider pores can be introduced by pressurization, which was not possible with conventional physical activation processes.

3.3.3 Particle and microdomain observation results

Figure 3-6 shows particle size distribution and mean particle sizes for each activated carbon. All activated carbon samples maintained the original spherical shape of the starting sample (carbonized BEAPS sample). For each activated carbon sample, P0.1T920, P0.5T900 and P1T870 had mean particle size of 4.9, 4.8, and 5.0 μm, respectively. There were almost no changes between pressurized conditions even though they had different degree of pore development. Also, particle size distribution showed the same tendency that 4–6 μm of particles were predominant regardless of the activation pressure.

Figure 3-7 shows microdomain images, microdomain size distribution and mean size of microdomain of prepared activated carbon samples estimated by using STM. P0.1T920 showed an unclear boundary between microdomains. By the pressurization, however, P0.5T900 and P1T870 showed clear boundary and spherical shapes. Microdomain distributions showed a shift to smaller size direction by pressurization. In addition, mean size of microdomains also showed a decreasing tendency: those of P0.1T920, P0.5T900, and P1T870 were 7.7 nm, 5.2 nm, and 4.8 nm, respectively. The STM results suggested two things; First thing is that inter-microdomain space was developed by pressurization, contributing the pore structure development. Second thing is that pressurization was not that effective for improving the intra-microdomain diffusion of activating agent as suggested from the decreased microdomain size by pressurization.

3.4 Conclusion

In Chapter 3, to investigate a possibility of the pressurized physical activation process, the gasification reactivity of the carbonized spherical phenol resin was evaluated under pressurized conditions using the MSB-TG apparatus. As a result, it was confirmed that the gasification reaction occurred at a lower temperature by pressurization. In other words, it was confirmed that the temperature required to achieve the same specific gasification rate decreased by pressurization. It was considered that pressurization improved the diffusibility of the activating agent gas and thus the gasification reaction, similar to the result seen in the pressurized stabilization in the carbon fiber manufacturing process in the previous study. In addition, as a result of evaluating the pore structure of activated carbons produced by atmospheric / pressurized physical activations, it was confirmed that the specific surface area greatly increased and the pore size distribution was also significantly changed by the pressurization. As a result of observing the microdomains of each sample, a difference in microdomain size was observed, which is presumed to be the cause of the change in the pore structure due to pressurization. On the other hand, since almost no change in the size of the particles was observed even when pressurized, it was considered that uniform activation was performed at the particle level. From these results, it was possible to confirm the pressurized physical activation was effective to prepare activated carbons with higher degree of pore development as compared with the conventional atmospheric physical activation.

Table 3-1. Temperatures to achieve the target gasification rate at different applied pressures.

	Achieved temperature at each pressure [^{o}C]		
Target gasification rate [%]	0.1 MPa	0.5 MPa	1.0 MPa
30	895	838	762
50	943	886	819
70	976	924	862

Table 3-2. Activation pressure, yield and pore structural parameters of the starting carbonized material (C6) and derived activated carbons prepared by atmospheric and pressurized physical activation methods.

Sample	Activation pressure [MPa]	Activation temperature [^{o}C]	Activation yield [%]	Specific surface area [m^2/g]	Total pore volume [cm^3/g]
P0.1T920	0.1	920	18	1140	0.6
P0.5T900	0.5	900	18	1910	1.3
P1T870	1.0	870	20	2680	1.5

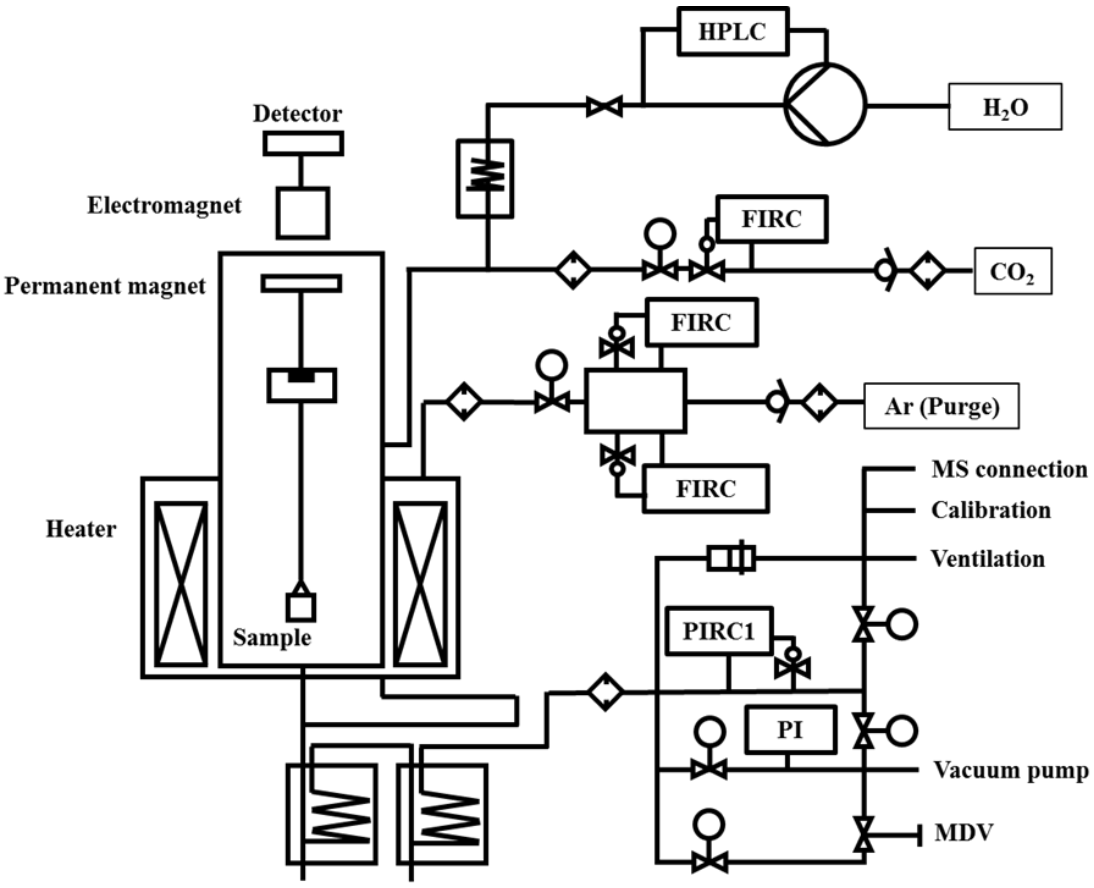

Figure 3-1. Schematic image of MSB-TG.

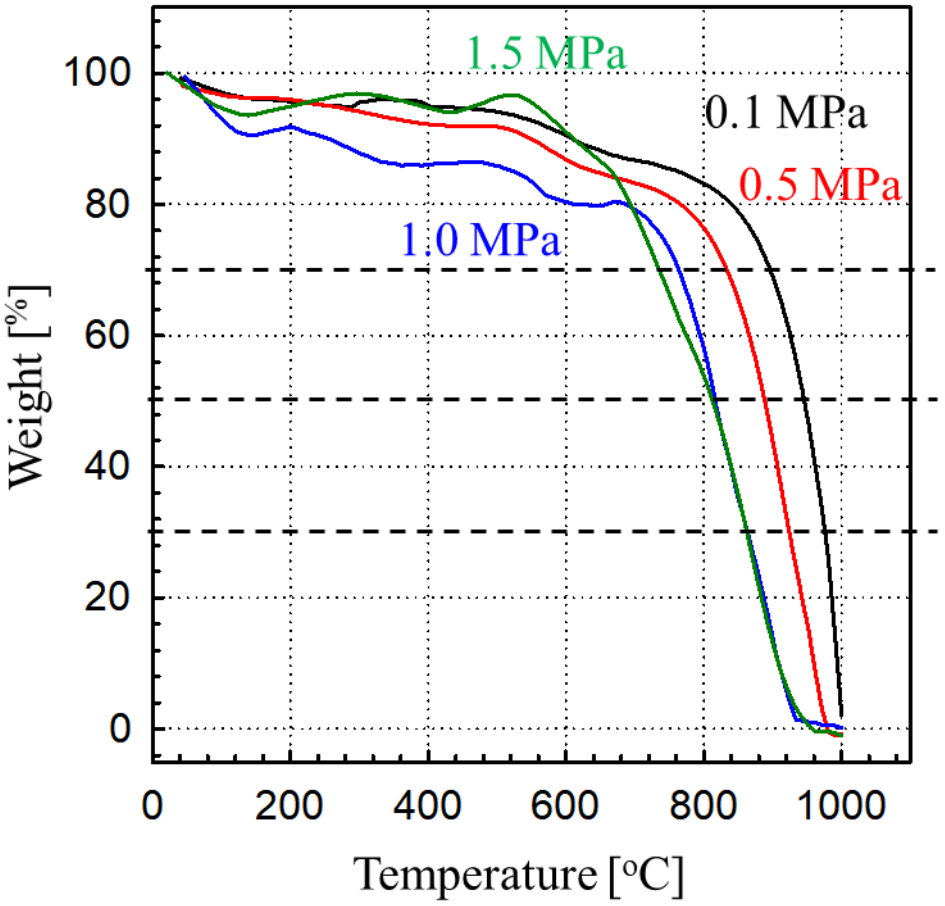

Figure 3-2. Pressurized thermogravimetric curves by MSB-TG at (black) 0.1, (red) 0.5, (blue) 1.0, and (green) 1.5 MPa of CO_2 pressure, respectively.

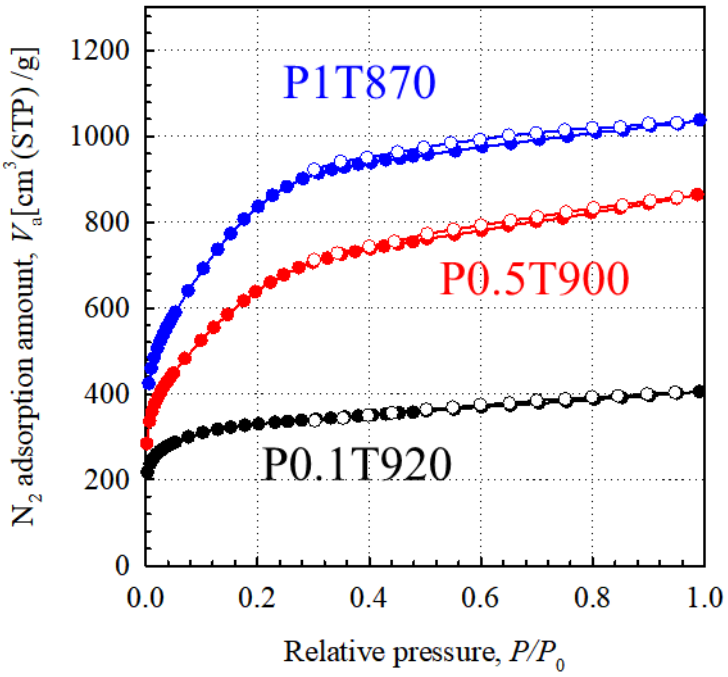

Figure 3-3. N_2 adsorption and desorption isotherms at 77 K of atmospheric and pressurized physical activated carbons. Solid and open symbols denote adsorption and desorption isotherms, respectively. (Black) P0.1T920; (red) P0.5T900; (Blue) P1T870. PXTY: X and Y indicate the activation pressure in MPa and temperature in degree Celsius, if any, respectively.

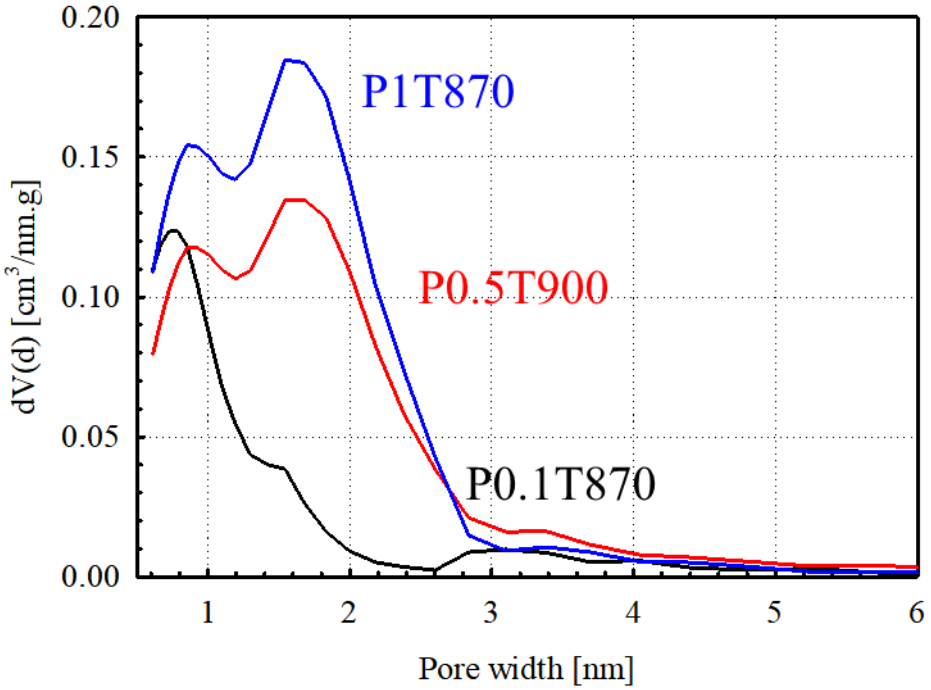

Figure 3-4. Pore size distributions for derived activated carbons. (Black) P0.1T920; (Red) P0.5T900; (Blue) P1T870.

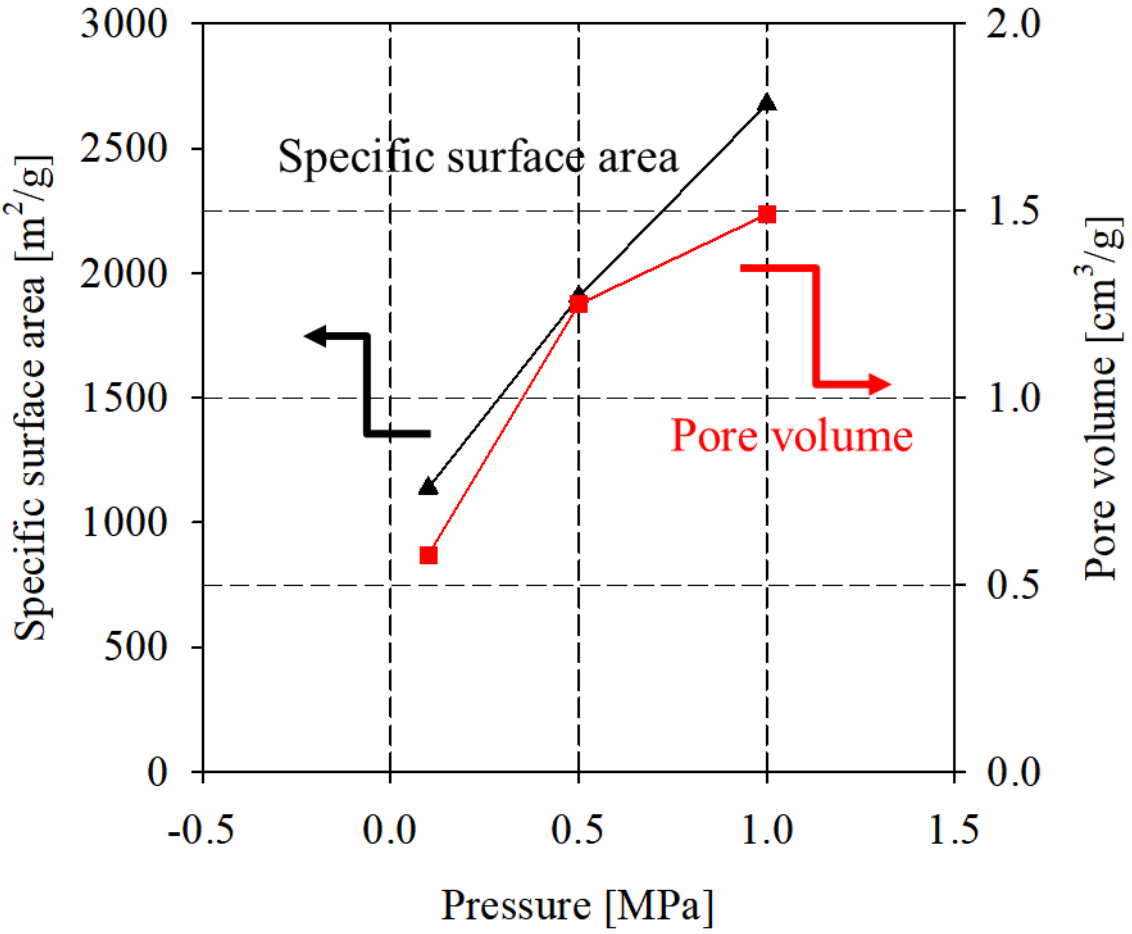

Figure 3-5. Changes of pore developments of activated carbons depending on the activation conditions. (Black) specific surface area and (red) total pore volume, respectively.

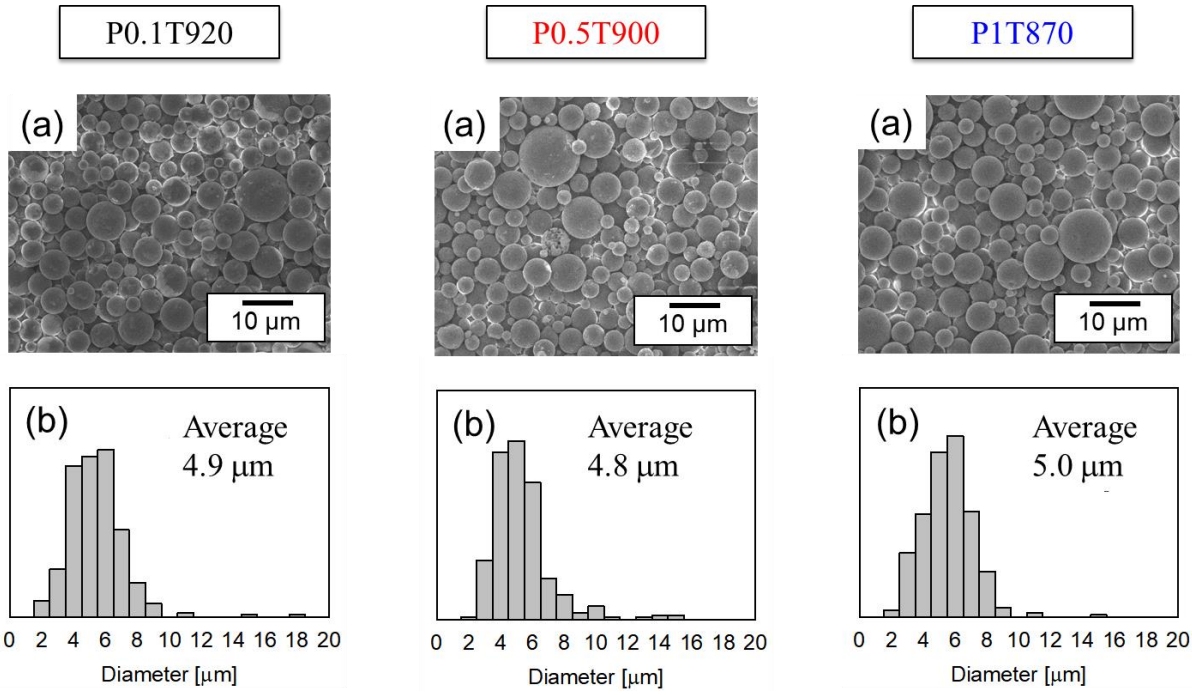

Figure 3-6. Scanning electron microscope (SEM) images and particle size distributions of activated carbons. (a) SEM image of P0.1T920 and its (b) distribution; (c) SEM image of P0.5T900 and its (d) distribution; (e) SEM image of P1T870 and its (f) distribution, respectively.

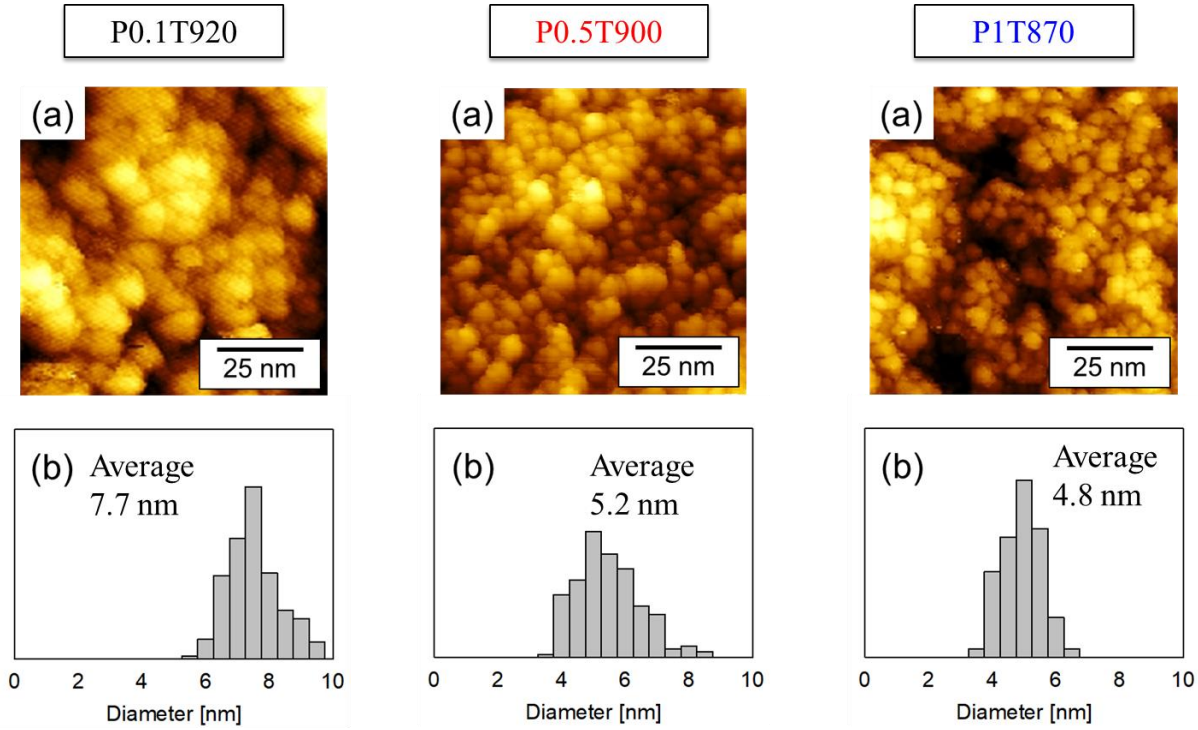

Figure 3-7. Scanning transmission electron microscope (STM) images and particle size distributions of activated carbons. (a) STM image of P0.1T920 and its (b) distribution; (c) STM image of P0.5T900 and its (d) distribution; (e) STM image of P1T870 and its (f) distribution, respectively.

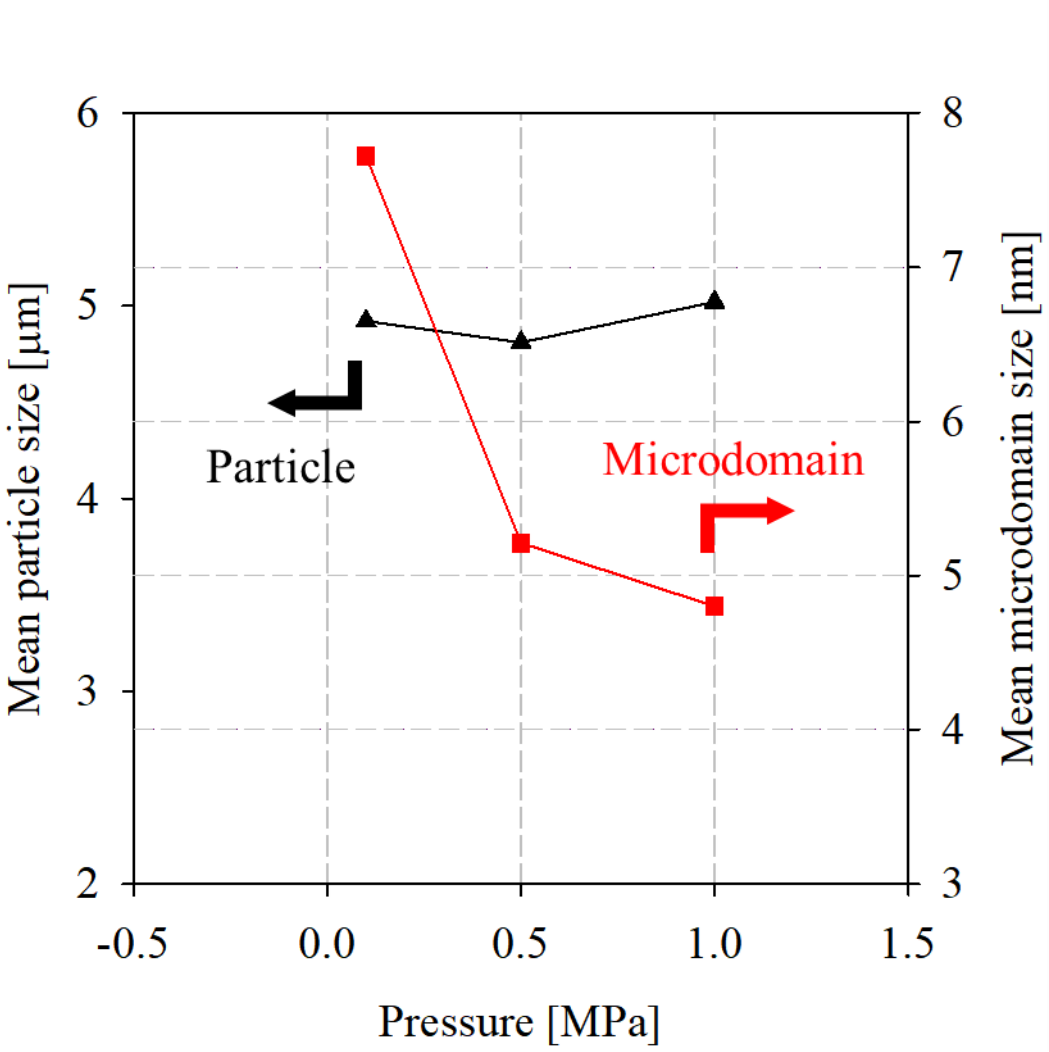

Figure 3-8. Relationship of activated carbon by each pressure to average particle or average microdomain size of activated carbons. (Black) average particle size and (red) average microdomain size, respectively.

Reference

[1] M. Molina-sabio, M. T. Gonzalez, F. Rodriguez-Reinoso, A. Sephijlveda-Escribano, Effect of steam and carbon dioxide activation in the micropore size distribution of activated carbon, *Carbon*, **33**, 1 (1995) 15–23.

[2] F. Rodriguez-Reinoso, M. Molina-sabio, M. T. Gonzalez, The use of steam and CO2 as activation agents in the preparation of activated carbons, *Carbon*, **34**, 4 (1996) 505–509.

[3] T. Otowa, Y. Nojima, T. Miyazaki, Development of KOH activation high surface area carbon and its application to drinking water purification, *Carbon*, **35**, 9 (1997) 1315–1319.

[4] T. Otowa, R. Tanibata, M. ltoh, Production and adsorption characteristics of MAXSORB: high-surface-area active carbon, *Gas Separation & Purification*, **7** (1993) 241–245.

[5] H. Shimanoe, S. Tanaka, T. Kotegawa, O. Kato, K. Nakabayashi, J. Miyawaki, S. -H. Yoon, Effect of pressurized oxidative stabilization on preparation of pitch-based carbon fiber. *Proceedings of The World Conference on Carbon (Carbon 2016)*, P4-35.

[6] H. Shimanoe, S. Ko, Y.-P. Jeon, K. Nakabayashi, J. Miyawaki, S.-H. Yoon, Shortening stabilization time using pressurized air flow in manufacturing mesophase pitch-based carbon fiber, *Polymers*, **11** (2019) 1911–1925.

[7] V. Liedtke, K. J. Hüttinger, Mesophase pitches as matrix precursor of carbon fiber reinforced carbon: I. Mesophase pitch preparation and characterization, *Carbon*, **34** (1996) 1057–1066.

[8] S. -S. Tzeng, P. -L. Wang, Oxidation of a petroleum pitch under pressure, *Carbon*, **39** (2001) 1103–1106.

[9] B. Fathollahi, B. Jones, P.C. Chau, J.L. White, Injection and stabilization of mesophase pitch in the fabrication of carbon–carbon composites. Part III: Mesophase stabilization at low temperatures and elevated oxidation pressures, *Carbon*, **43** (2005) 143–151.

[10] K. Kaneko, C. Ishii, M. Ruike, H. Kuwabara, Origin of superhigh surface area and microcrystalline graphitic structures of activated carbons, *Carbon*, **30** (1992) 1075–1088.

[11] A. V. Neimark, Y. Lin, P. I. Ravikovitch, M. Thommes, Quenched solid density functional theory and pore size analysis of micro-mesoporous carbons, *Carbon*, **47** (2009) 1617–1628.

Chapter 4.

Effect of pressurization on activated carbon manufacturing process

Pressurized physical activation: A simple production method for activated carbon with a highly developed pore structure (H. Yi, *et al.*, *Carbon*, **183** (2021) 735–742.)

4.1 Introduction

Activated carbon is a useful artificial material; because of its developed pore structure, it has been adopted as an adsorbent for air and water purification [1–3], gas separation [4, 5], catalyst carrier [6], and electrode materials for energy storage devices [7–9]. To improve its performance and exploit new application fields, there is a need to increase the degree of pore development in activated carbon. The process of developing a pore structure in carbon is known as activation, which is divided into physical and chemical methods. Physical activation methods were developed earlier and are more widely used in industry; they can manufacture activated carbon with a low cost because of the lower activating agent price (e.g., steam, CO_2, or air) and lack of requirements for subsequent treatment and special facilities [9–12]. However, the limited extent of pore development and comparatively low activation yield are disadvantages of such methods. Chemical activation methods involve the use of substances such as $ZnCl_2$, phosphate, and alkali metal compounds as activating agents to manufacture activated carbon, thereby providing more highly developed pore structures and higher yields [2, 13–16]. However, these chemical activation methods inevitably require a post-treatment acid-washing process to remove the residues of the chemical activating agent and are therefore costly.

Recently, trials to obtain activated carbon with highly developed pores have been conducted and various methods have been proposed [17–20]. However, these methods are based on chemical activation; high production costs remain problematic. Thus, there is a need to develop a simple production method for activated carbon with highly developed pores, comparable with the results of chemical activation, but with low production costs, similar to the costs of physical activation methods.

In our previous work, our research group have reported the existence of microdomains as a basic structural unit of artificial carbon materials and proposed a microdomain structure model to describe the pore structure of activated carbon [21]. Based on this microdomain structure model, our research group have elucidated the differences between physical and chemical activation mechanisms [22]. Chemical activation provides widespread uniform pore development for microdomains comprising carbon particles, whereas physical activation causes inhomogeneous gasification from the outer surface of the carbon particles and their microdomains, thereby producing a lower degree of pore development and lower activation yield. These findings suggested that, during physical activation, the activating agent molecules preferentially react with solid carbon on the outer surfaces of particles and microdomains, prior to penetration into core areas. Therefore, if the activating agent diffusibility can be improved, a more homogenous activation reaction could be achieved for all microdomains within each carbon particle. Thus, highly developed pores and a high activation yield could be obtained even by physical activation.

Here, our research group would like to suggest the pressurization may aid in increasing the activation agent diffusibility; our research group have reported in a study of the stabilization process of carbon fiber production [23] that pressurization improved the oxygen gas

diffusibility, resulting in a homogenous stabilization reaction throughout pitch fibers. Positive influence of pressurization on pyrolytic and gasification performances of carbonaceous materials has been also reported [24-36]. In pyrolysis, for example, some studies have shown the increase of char yield by pressurization [24, 28]. Also, pressurization was found to accelerate the gasification reaction of chars [30–35]. Zhang *et al.* have reported an increase of surface area and pore volume by pressurization, but this study did not discuss the pore development mechanism by pressurization [29]. In Chapter 4, I propose a novel pressurized physical activation method as a simple production process for activated carbon with a highly developed pore structure.

4.2 Experimental

4.2.1 Sample preparation

As a raw material, carbonized 8 μm spherical phenol resin was used also in Chapter 4 as in Chapter 3. The carbonized material (C6) was heated to 700−900°C at a rate of 5 °C/min in a flow (150−200 cm^3/min) of pure CO_2 at a pressure of 0.1 or 1.0 MPa for atmospheric or pressurized activation, respectively, without holding. To obtain activated carbon with a higher degree of activation, portions of C6 were held at 900℃ in the CO_2 flow for various intervals. The obtained activated carbons were designated as PXTYmZ, where X, Y, and Z indicate the activation pressure, temperature, and holding time at 900℃, if any, respectively; for example, P0.1T900m15 indicates activated carbon prepared at 0.1 MPa and 900℃ and held for 15 min. Activation yield was calculated by the following equation.

$$\text{Activation yield [\%]} = \frac{\text{Weight after activation [g]}}{\text{Weight before activation [g]}} \times 100 = 100 - \text{Burn-off [\%]}$$

4.2.2 Characterization

To investigate pore characteristics, I measured N_2 adsorption and desorption isotherms at 77 K using a surface area analyzer (Nova-e series; Anton Paar QuantaTec Inc., USA). Pore structural parameters including total pore volume and specific surface area were calculated by the α_S-plot [37] and quenched solid density functional theory (QSDFT) [38] methods from the N_2 adsorption isotherms. The porosity was calculated as

$$\text{Porosity}\left[\frac{\text{cm}^3}{\text{cm}^3}\right] = \text{Total pore volume}\left[\frac{\text{cm}^3}{\text{g}}\right] \times \text{Bulk density}\left[\frac{\text{g}}{\text{cm}^3}\right]$$

where bulk density was estimated by packing each specimen in a cylinder having an inner diameter of 1.6 mm and a depth of 2.5 mm.

Particle size was determined using a scanning electron microscope (SEM, JSM-6700F; JEOL, Japan), evaluating the mean size of 300 particles in SEM images of each sample. To investigate the microdomain size and structure, I also acquired scanning tunneling microscope (STM, Agilent Technologies 5500 Scanning Probe Microscope; Toyo Corporation, Japan) images, using its constant current mode (current: 0.3‑1.2 nA, bias voltage: 0.1–1.5 V, and scan frequency: 1–2 Hz).

4.3 Results and discussion

4.3.1 Pore structure evaluations of activated carbon

Figure 4-1 shows the N_2 adsorption and desorption isotherms at 77 K of the starting carbonized material (C6) and activated carbon derived from both the atmospheric and pressurized physical activation methods, with CO_2 as the activating agent. The activation yields and pore structural parameters calculated by the α_S-plot method from N_2 adsorption isotherms are listed in **Table 4-1**. For all forms of activated carbon, adsorption hysteresis originating from mesopores was nearly undetectable. At an activation pressure of 0.1 MPa, there were no significant differences in the yield or N_2 adsorption isotherms for activation temperatures up to 800℃. At 900℃, however, the adsorption amount of N_2 increased in the low relative pressure (P/P_0) region, with a noticeable decrease of the activation yield. By holding the specimen at 900℃, activation progressed: P0.1T900m90 exhibited a specific surface area of 1650 m^2/g, total pore volume of 0.59 cm^3/g, and activation yield of 13%. In contrast, when physical activation was performed at a CO_2 pressure of 1.0 MPa, a remarkable increase in N_2 adsorption was observed even at an activation temperature of 800℃, and further pore development was confirmed at 900℃. As shown in **Table 4-1**, lower activation yields were observed for pressurized activated carbon than for atmospheric activated carbon at the same activation temperature and holding time. Indeed, pressurization reportedly increases the rate of conversion of char particles into CO gas during CO_2 gasification [31, 32, 35]. However, the much higher specific surface area and total pore volume of pressurized activated carbon suggest that the pressurization should have enhanced CO_2 diffusibility into carbon particles and/or microdomains to efficiently develop pores. The highest degree of pore development was obtained for P1T900m5 (specific surface area: 2630 m^2/g and total pore volume: 1.31 cm^3/g)

at 12% yield. At 1.0 MPa and 900℃, the longer activation period of 15 min (P1T900m15) induced complete gasification and activated carbon was not obtained.

Figure 4-2 shows the pore size distribution of activated carbon, calculated by the QSDFT method. CO_2 activation at 0.1 MPa was found to preferentially introduce narrow micropores less than 1.0 nm of pore width. A longer activation period at 900℃ developed comparatively wide micropores (1.0–1.5 nm) in atmospheric activated carbon (P0.1T900m15 and P0.1T900m90). In contrast, activation at 1.0 MPa resulted in the development of 1.0–1.5 nm wide pores even at an activation temperature of 800℃ (P1T800). The pore size distribution was gradually broadened with increases of the activation temperature and holding time; P1T900m5 exhibited a prominent peak for a pore width of about 1.6 nm, indicating a development of wide micropores at that width and corresponding to a significant increase in the total pore volume of this activated carbon.

The relationships of activation yield with specific surface area and total pore volume are shown in **Figure 4-3**. These confirm an apparent difference between the atmospheric (0.1 MPa) and pressurized (1.0 MPa) physical activations: The gradient of the degree of pore development compared with activation yield was much steeper for the pressurized activated carbon than for the atmospheric activated carbon. This led to considerable differences in specific surface area and total pore volume at a similar yield, indicating the effectiveness of pressurization for pore development. Notably, pressurized physical activation yielded a specific surface area of 2630 m^2/g, which is difficult to achieve by conventional atmospheric physical activation. For a similar level of pore development, a higher activation yield was obtained for the pressurized activated carbon (e.g., 53% vs. 21% for pressurized and atmospheric activated carbon, respectively, at a specific surface area of approximately 1400 m^2/g). From the perspective of

activation yield, pressurization can suppress the unwanted local gasification of solid carbon, causing more efficient pore development.

In addition, the relationships of activation yield from carbonized BEAPS, so-called char, to degree of pore development tendency are shown in **Figure 4-4**. The specific surface area per char weight was reduced by the pressurization, indicating that the gasification without pore development was suppressed. In addition, to the total pore capacity per char weight, it was confirmed that same tendency with specific surface area per char weight. From **Figure 4-4**, pore development degree vs. char weight results are shown that the inefficient gasification reaction was restrained by pressurization, which contributed to the higher yield and pore structure development degree.

Changes of bulk density and porosity with the degree of activation are shown in **Figure 4-5**. With a decrease of activation yield, in other words, with a progress of activation, the bulk density decreased regardless of the activation pressure (**Figure 4-5(a)**). However, the pressurization induced the more decrease of bulk density, which was attributed to the higher degree of pore development: As shown in **Figure 4-5(b)**, a noticeable difference of porosity of atmospheric and pressurized activated carbon samples confirmed the effectiveness of pressurization for pore development.

4.3.2 Particle and microdomain observations of activated carbon

Figure 4-6 and **Figure 4-7** show SEM images of atmospheric and pressurized physically activated carbons, respectively. All activated carbon samples maintained a spherical shape. **Figure 4-8** shows the change in mean particle size with activation yield and the particle size

distributions for atmospheric and pressurized activated carbon. In atmospheric activated carbon, mean particle size decreased with increasing degree of activation (**Figure 4-8(a)**) and the particle size distribution tended to shift leftward (**Figure 4-8(b)**). This decrease in size agrees with our previous findings for atmospheric physical activation using steam as an activating agent [22]. In contrast, pressurized activated carbon showed no change in either mean particle size (**Figure 4-8(a)**) or particle size distribution (**Figure 4-8(c)**). When considered together with the porosity assessment results, these findings indicate that pressurization can achieve a uniform reaction, at least at the particle level.

To compare the changes in microdomain structure under atmospheric and pressurized physical activations, I applied STM technique to P0.1T900m90 and P1T900m5 as representatives of atmospheric and pressurized activated carbon, respectively, with similar activation yields. The resulting images and microdomain size distributions are shown in **Figure 4-9**. P0.1T900m90 showed an unclear boundary between microdomains; however, P1T900m5, obtained by pressurized physical activation, showed a clear boundary. The distributions indicated that the microdomains tended to be smaller in P1T900m5 than in P0.1T900m90; the mean microdomain sizes were 5.0 and 6.1 nm for the pressurized and atmospheric activated carbon, respectively. The STM results suggested that pressurization was ineffective for improving activating agent diffusion into microdomains.

4.3.3 Pore development mechanism of pressurized physical activation

Figure 4-10 shows a schematic model of the mechanistic difference in pore development of the atmospheric physical, pressurized physical, and chemical activation methods based on the microdomain structure model [21]. According to the model, a carbon particle consists of

numerous microdomains, and both inter- and intra-microdomain spaces function as pores. During chemical activation, sizes of carbon particles and microdomains do not show noticeable changes regardless of the degree of activation, indicating a sufficient diffusibility of the activating agents in both carbon particles and microdomains. This enables uniform reaction of the activating agents with each microdomain in the carbon particle, and both inter- and intra-microdomain pores are well developed [22]. For conventional atmospheric physical activation, on the other hand, the low activating agent diffusibility causes local gasification reactions at the outer surfaces of microdomains and carbon particles, causing decreases in size of both carbon particles and microdomains. This results in the low activation yield and degree of pore development observed under atmospheric physical activation [39–41]. In contrast, the diffusion at the particle level was improved in pressurized activated carbon in this study, as revealed by the unchanged particle size even at the high degree of activation (**Figure 4-8**). Previous studies [23, 42] have reported that gas diffusibility in solid carbon materials can be improved by pressurization. However, the decrease of microdomain size suggested little influence of the pressurization on the improvement of the activating agent diffusibility. Therefore, the remarkable increases in specific surface area and total pore volume under pressurization can presumably be attributed to the development of inter-microdomain pores. That is, the pressurized physical activation method can produce a high degree of pore development, between the development outcomes achieved by chemical and atmospheric physical activation methods.

4.4 Conclusion

To produce activated carbon with a highly developed pore structure by a simple production process, a novel pressurized physical activation method was proposed. It was found that the pressurized activated carbon achieved either a higher degree of pore development for a similar activation yield or a higher activation yield for a similar degree of pore development. Furthermore, a characteristic pore size distribution, with a maximum at approximately 1.6 nm, was obtained by pressurization. Observation results of particles and microdomains revealed that pressurization improved the diffusibility of activation agent into carbon particles, but not in their microdomains. Consequently, I successfully demonstrated the effectiveness of the pressurized physical activation method to produce activated carbon with a high degree of pore development by means of improving diffusibility of activating agent at the particle level.

Table 4-1. Activation yield and pore structural parameters of the starting carbonized material (C6) and derived activated carbons prepared by atmospheric and pressurized physical activation methods.

Sample	Activation pressure [MPa]	Activation yield [%]	Total pore volume [cm^3/g]	Specific surface area [m^2/g]
C6	-	-	0.18	570
P0.1T700	0.1	86	0.18	570
P0.1T800		82	0.18	590
P0.1T900		66	0.32	1020
P0.1T900m5		44	0.36	1150
P0.1T900m15		21	0.49	1410
P0.1T900m90		13	0.59	1650
P1T700	1.0	78	0.24	760
P1T800		53	0.46	1390
P1T900		40	0.65	1940
P1T900m5		12	1.31	2630
P1T900m15		0	-	-

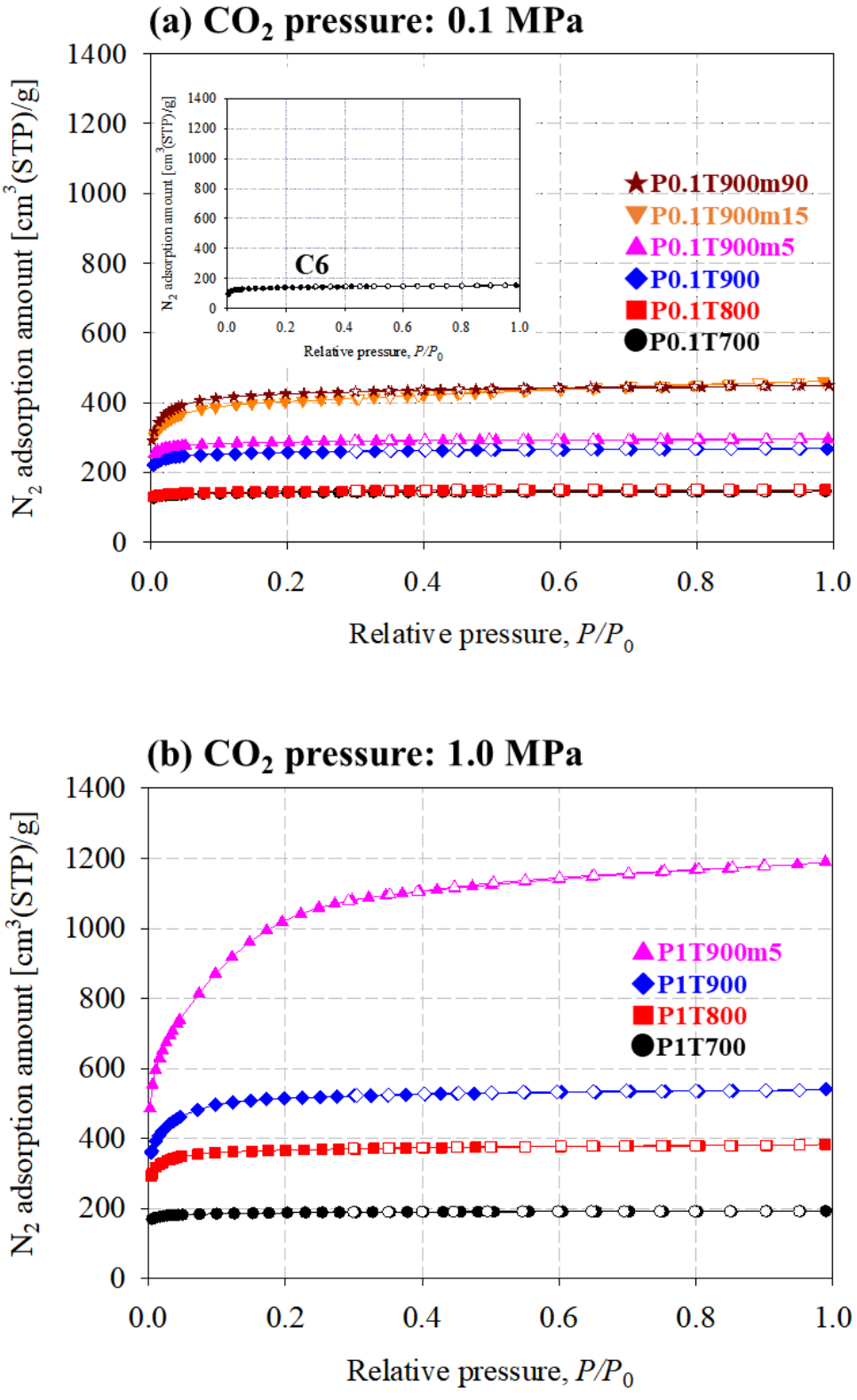

Figure 4-1. N_2 adsorption and desorption isotherms at 77 K of atmospheric physical activated

carbons. Solid and open symbols denote adsorption and desorption isotherms, respectively. (Circle) P0.1T700 or P1T700; (square) P0.1T800 or P1T800; (rhombus) P0.1T900 or P1T900; (triangle) P0.1T900m5 or P1T900m5; (inverted triangle) P0.1T900m15; and (star) P0.1T900m90. PXTYmZ: X, Y, and Z indicate the activation pressure, temperature, and holding time at 900℃, if any, respectively. Inset: The results of the starting carbonized material (C6) are shown for comparison.

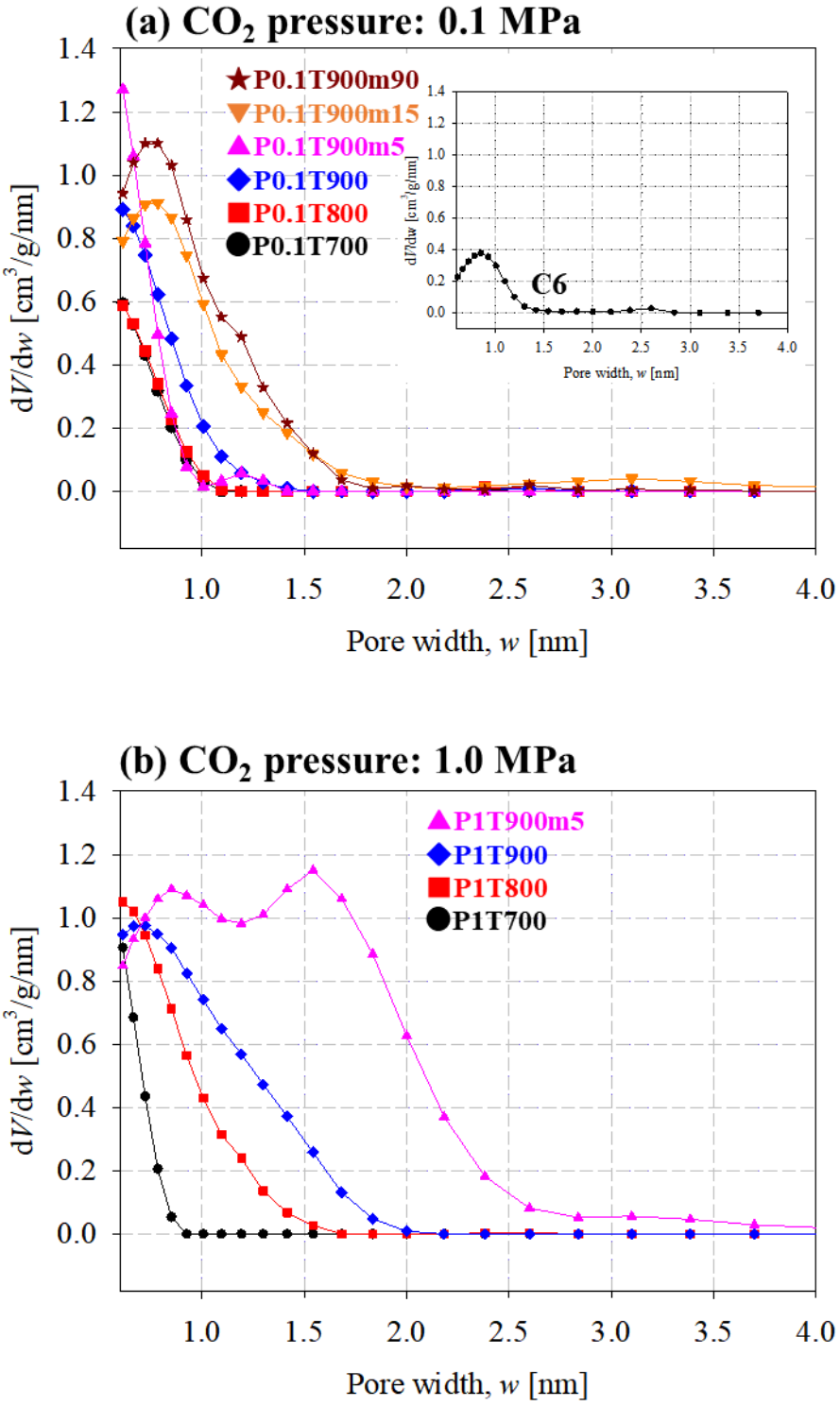

Figure 4-2. Pore size distributions of atmospheric physical activated carbons. (Circle) P0.1T700 or P1T700; (square) P0.1T800 or P1T800; (rhombus) P0.1T900 or P1T900; (triangle) P0.1T900m5 or P1T900m5; (inverted triangle) P0.1T900m15;

and (star) P0.1T900m90. Inset: The results of the starting carbonized material (C6) are shown for comparison.

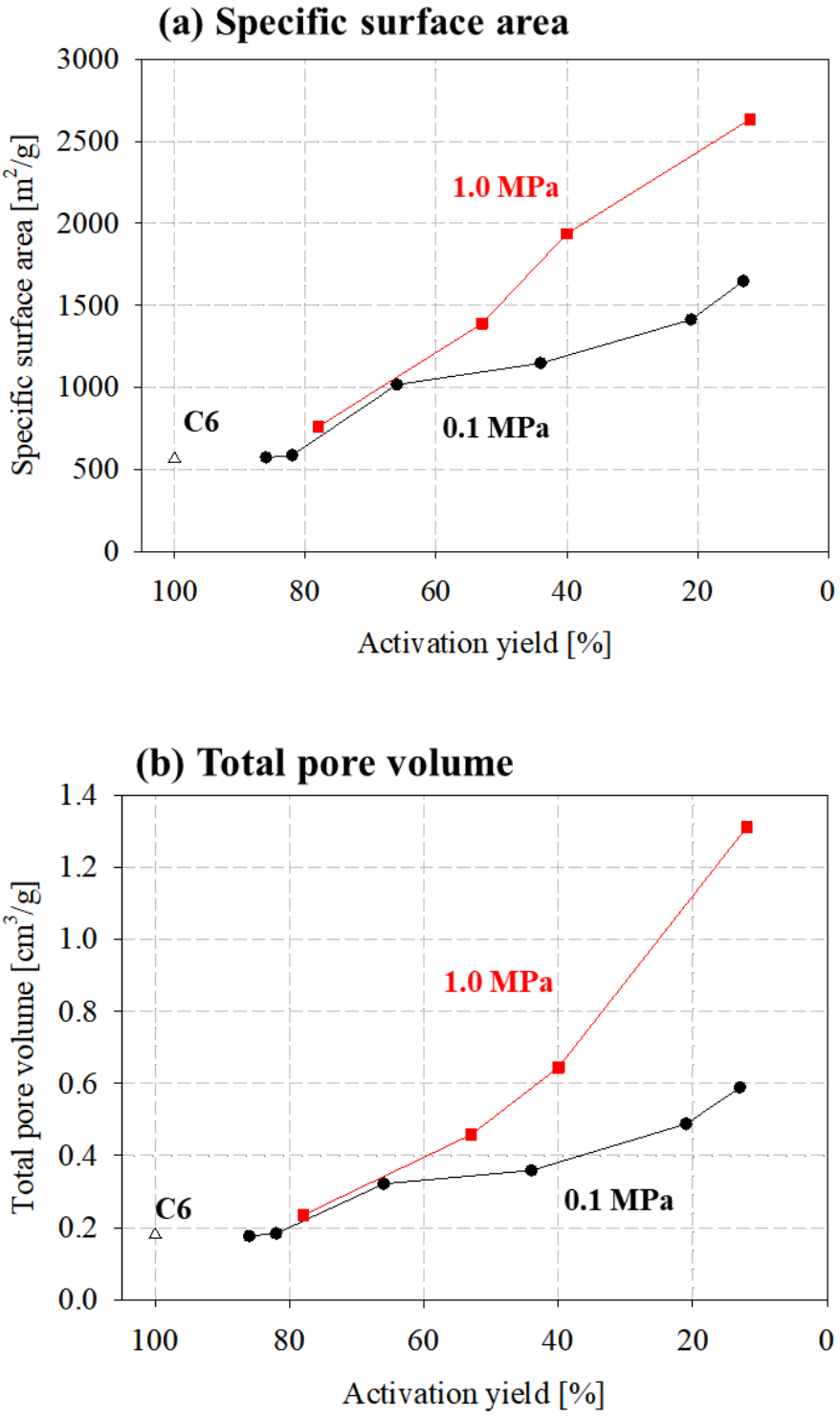

Figure 4-3. Relationship of activation yield to degree of pore development for activated carbons prepared by (black circle) atmospheric and (red square) pressurized physical activation methods with CO_2 as an activating agent: (a) yield vs. specific

surface area; (b) yield vs. total pore volume. The results of the starting carbonized material (C6; open triangle) are shown for comparison.

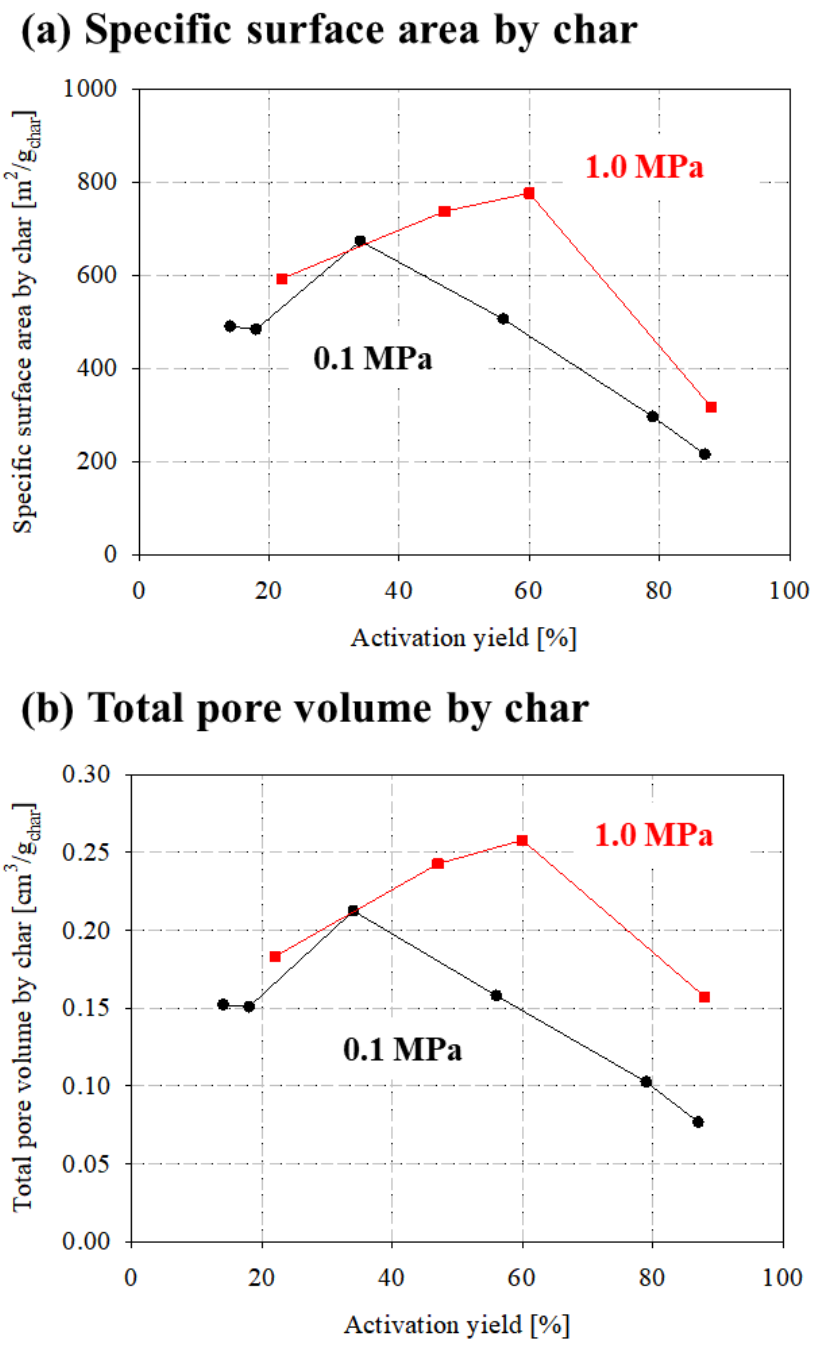

Figure 4-4. Relationship of activation yield to degree of pore development for activated carbons prepared by (black circle) atmospheric and (red square) pressurized physical activation methods with CO_2 as an activating agent: (a) activation yield rate vs. specific surface area by char; (b) activation yield vs. total pore volume by char.

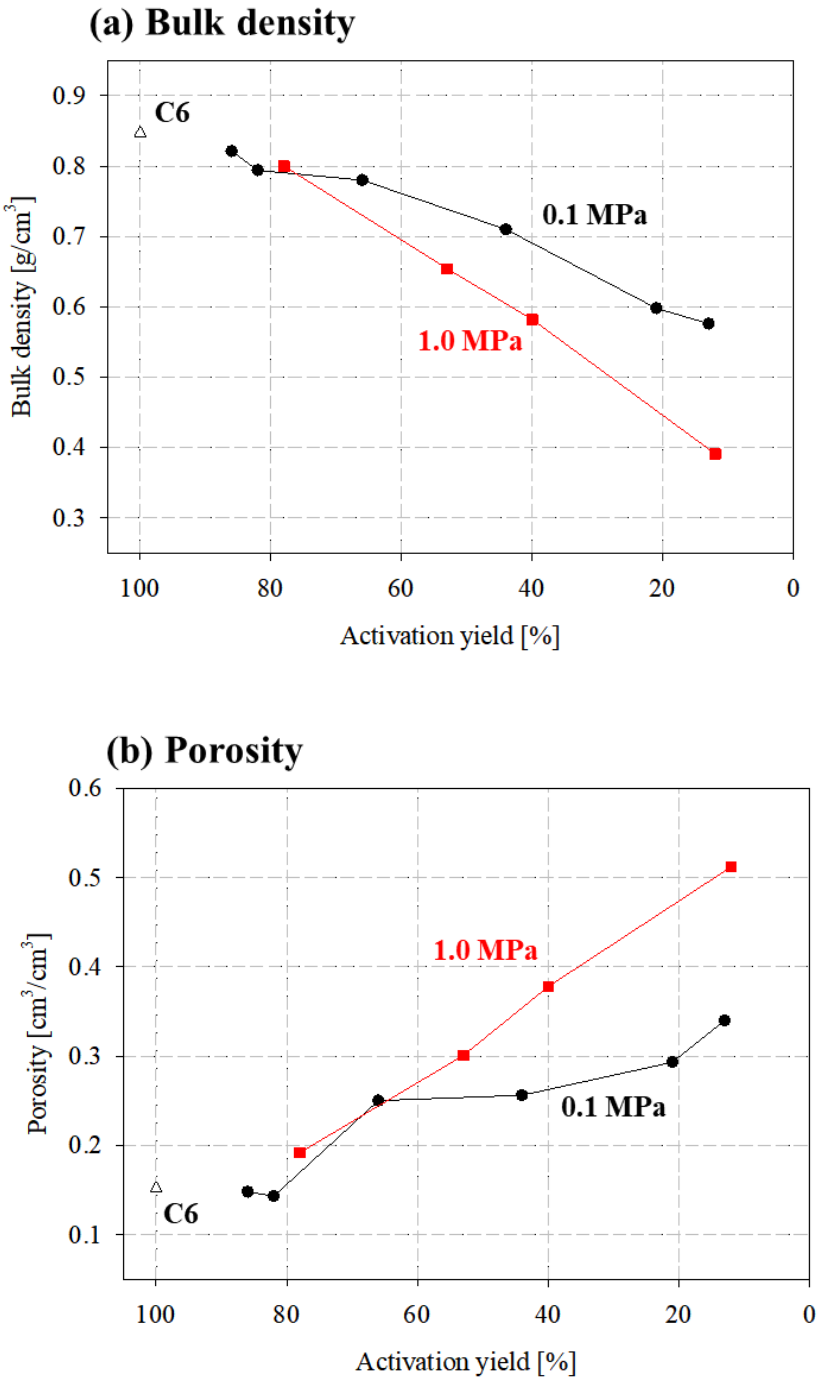

Figure 4-5. Relationships of activation yield to (a) bulk density and (b) porosity for activated carbons prepared by (black circle) atmospheric and (red square) pressurized physical activation methods. The results of the starting carbonized material (C6; open triangle) are shown for comparison.

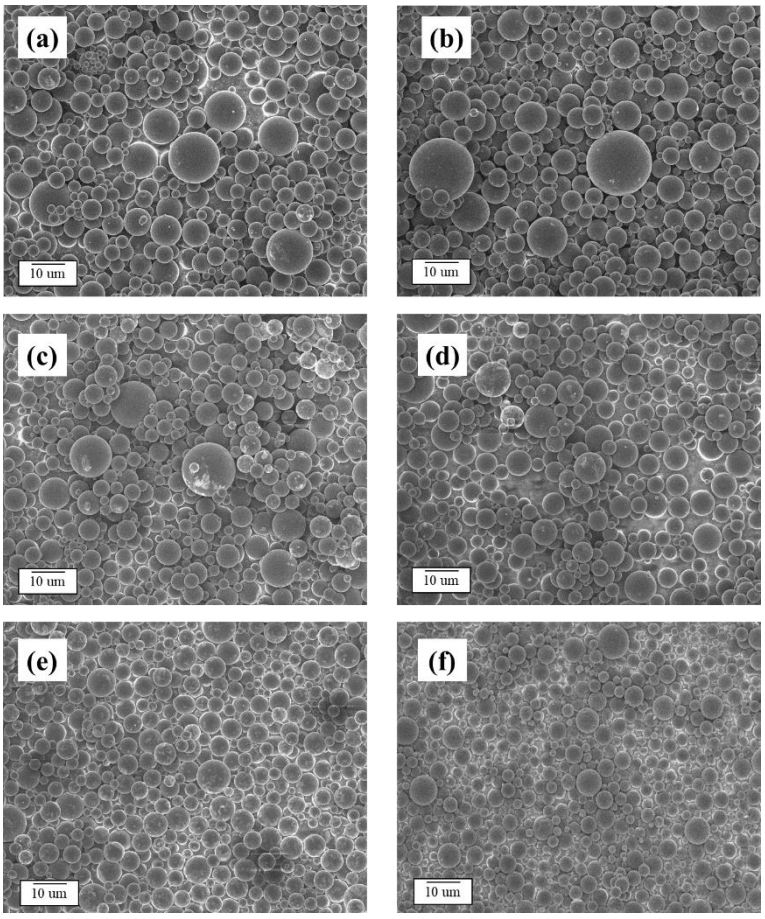

Figure 4-6. Scanning electron microscope (SEM) images of activated carbons prepared by atmospheric physical activation. (a) P0.1T700; (b) P0.1T800; (c) P0.1T900; (d) P0.1T900m5; (e) P0.1T900m15; (f) P0.1T900m90. PXTYmZ: X, Y, and Z indicate the activation pressure, temperature, and holding time at 900℃, if any, respectively.

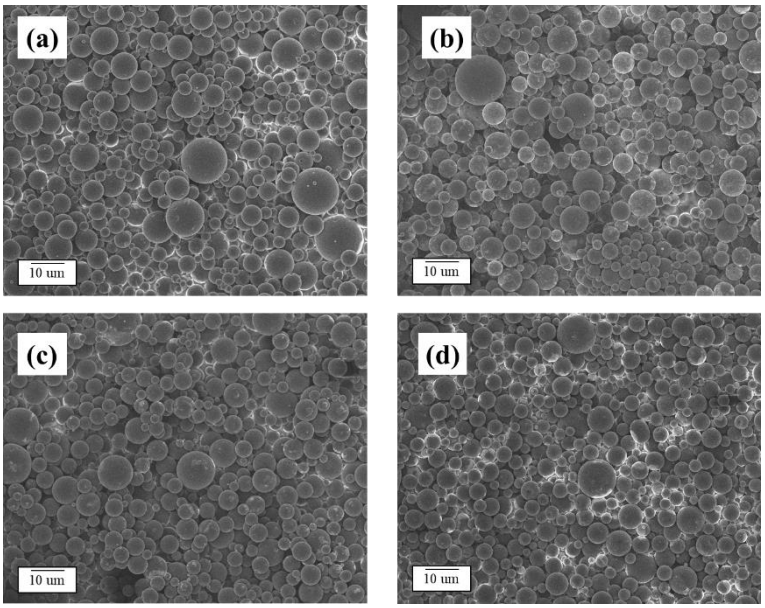

Figure 4-7. SEM images of activated carbons prepared by pressurized physical activation at 1.0 MPa of CO_2 pressure. (a) P1T700; (b) P1T800; (c) P1T900; (d) P1T900m5.

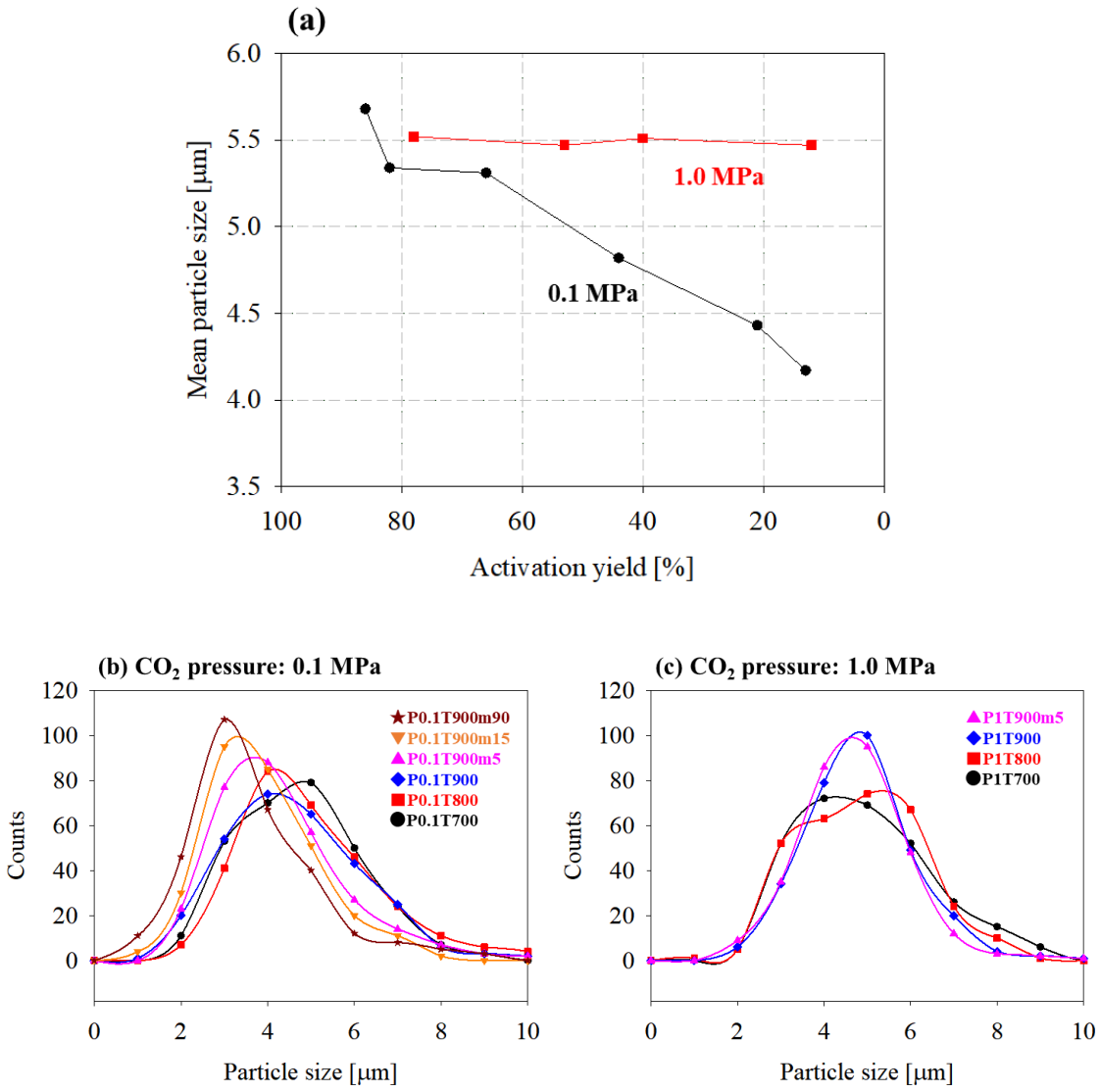

Figure 4-8. (a) Relationships between mean particle size and activation yield for atmospheric (black, circle) and pressurized physical activations (red, square), and particle size distributions of (b) atmospheric and (c) pressurized physical activated carbons. (Circle) P0.1T700 or P1T700; (square) P0.1T800 or P1T800; (rhombus) P0.1T900 or P1T900; (triangle) P0.1T900m5 or P1T900m5; (inverted triangle) P0.1T900m15; and (star) P0.1T900m90.

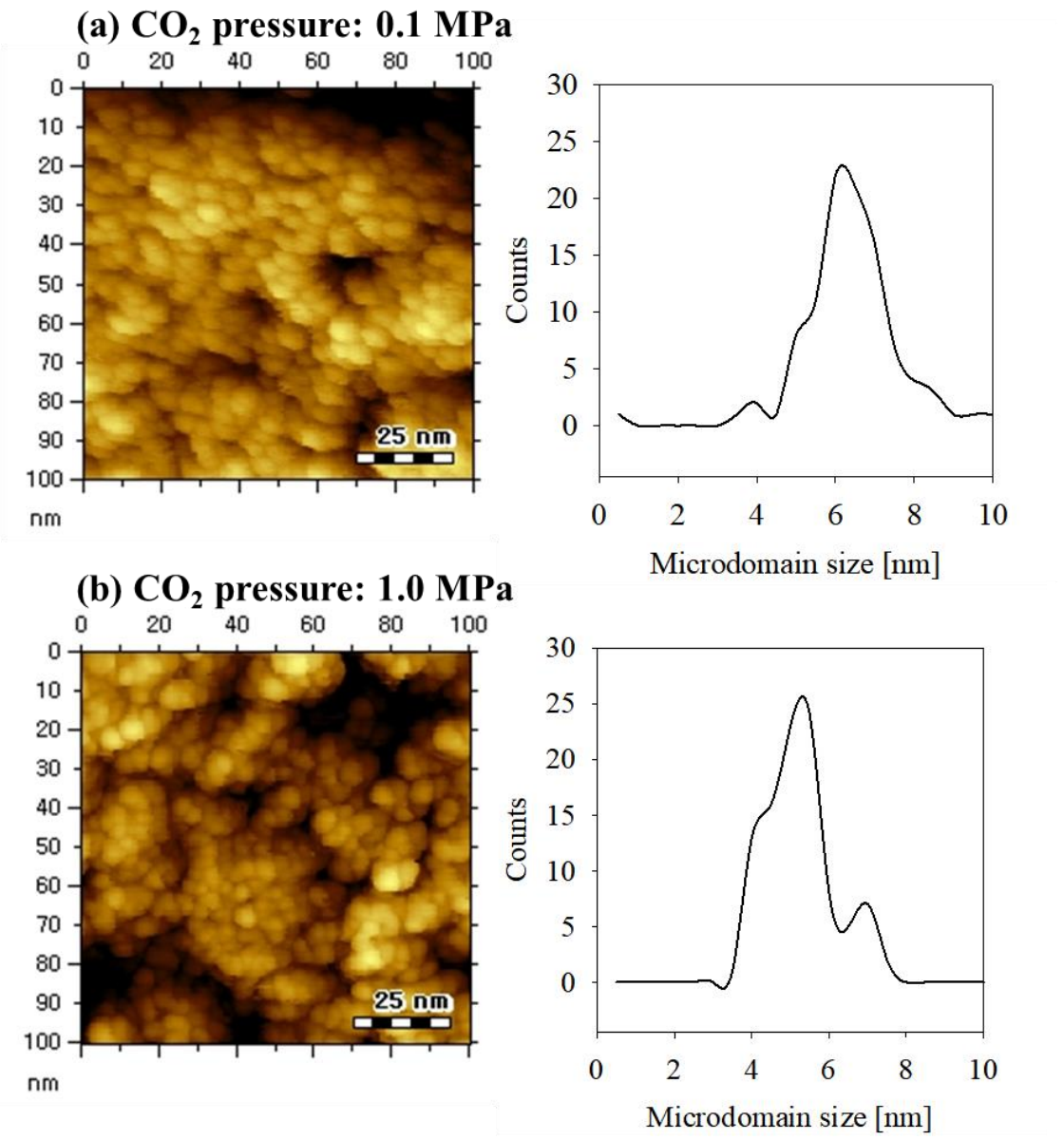

Figure 4-9. STM images and microdomain size distributions of (a) P0.1T900m90 and (b) P1T900m5.

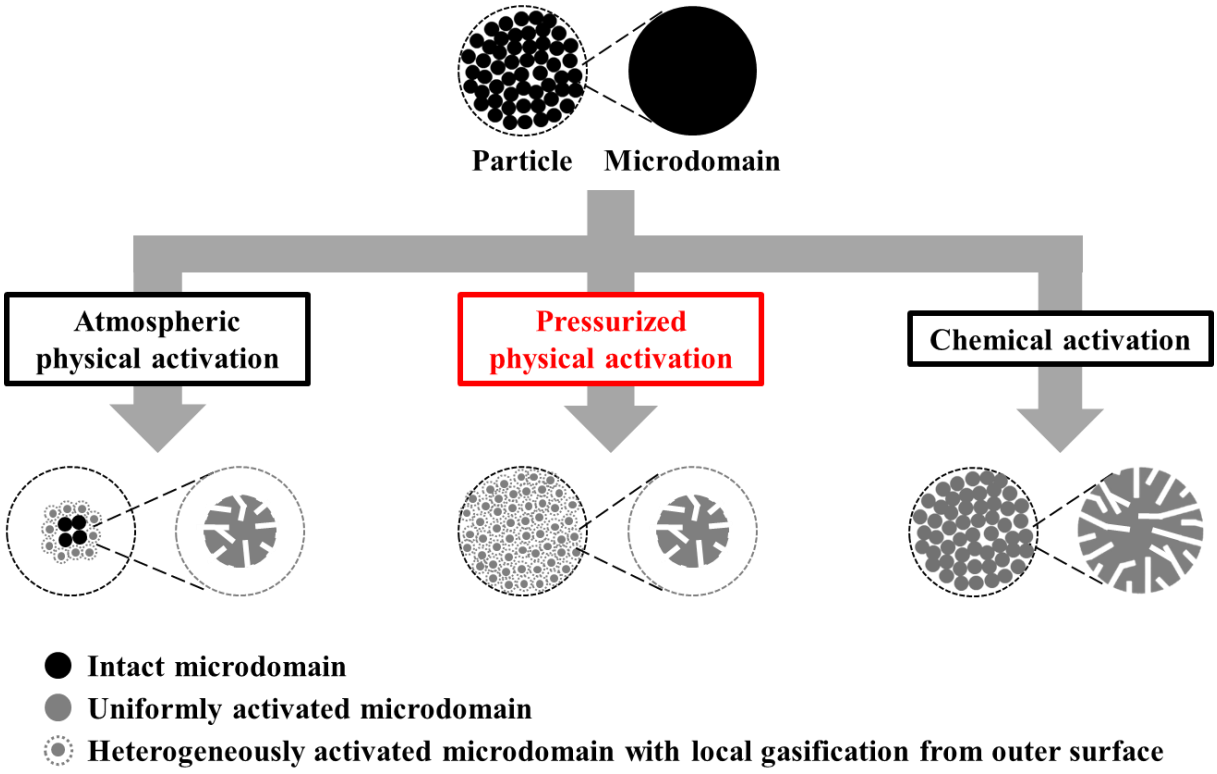

Figure 4-10. Schematic diagram of differences in atmospheric physical, pressurized physical, and chemical activation processes.

References

[1] I. Langmuir, The adsorption of gases on plane surfaces of glass mica and platinum, *J. Am. Chem. Soc.*, **40**, 9 (1918) 1361–1403.

[2] T. Otowa, Y. Nojima, T. Miyazaki, Development of KOH activated high surface area carbon and its application to drinking water purification, *Carbon*, **35**, 9 (1997) 1315–1319.

[3] D. Mohan, C. U. Pittman, Arsenic removal from water/wastewater using adsorbents—A critical review, *J. Hazard. Mater.*, **142**, 1–2 (2007) 1–53.

[4] S. Sircar, T. C. Golden, M. B. Rao, Activated carbon for gas separation and storage, *Carbon*, **34**, 1 (1996) 1–12.

[5] K. T. Chue, J. N. Kim, Y. J. Yoo, S. H. Cho, Comparison of activated carbon and zeolite 13X for CO_2 recovery from flue gas by pressure swing adsorption, *Ind. Eng. Chem. Res.*, **34**, 2 (1995) 591–598.

[6] Z. Liu, X. Y. Ling, X. Su, J. Y. Lee, Carbon-supported Pt and PtRu nanoparticles as catalysts for a direct methanol fuel cell, *J. Phys. Chem. B*, **108**, 24 (2004) 8234–8240.

[7] E. Frackowiak, F. Béguin, Carbon materials for the electrochemical storage of energy in capacitors, *Carbon*, **39**, 6 (2001) 937–950.

[8] Y. Zhai, Y. Dou, D. Zhao, P. F. Fulvio, R. T. Mayes, S. Dai, Carbon materials for chemical capacitive energy storage, *Adv. Mater.*, **23**, 42 (2011) 4828–4850.

[9] F. Rodríguez-Reinoso, M. Molina-Sabío, M. T. González, The use of steam and CO_2 as activating agents in the preparation of activated carbons, *Carbon*, **33**, 1 (1995) 15–23.

[10] M. Molina-Sabio, M. T. González, F. Rodriguez-Reinoso, A. Sepúlveda-Escribano, Effect of steam and carbon dioxide activation in the micropore size distribution of activated carbon, *Carbon*, **34**, 4 (1996) 505–509.

[11] T. Zhang, W. P. Walawender, L. T. Fan, M. Fan, D. Daugaard, R. C. Brown, Preparation

of activated carbon from forest and agricultural residues through CO_2 activation. *Fuel*, **105**, 1–2 (2004) 53–59.

[12] M. Yu, Y. Han, J. Li, L. Wang, CO_2-activated porous carbon derived from cattail biomass for removal of malachite green dye and application as supercapacitors, *Chem. Eng. J.*, **317** (2017) 493–502.

[13] J. Wang, S. Kaskel, KOH activation of carbon-based materials for energy storage, *J. Mater. Chem.*, **22** (2012) 23710–23725.

[14] T. Otowa, R. Tanibata, M. ltoh, Production and adsorption characteristics of MAXSORB: High-surface-area active carbon, *Gas Sep. Purif.*, **7**, 4 (1993) 241–245.

[15] M. A. Lillo-Ródenas, D. Cazorla-Amorós, A. Linares-Solano, Understanding chemical reactions between carbons and NaOH and KOH: An insight into the chemical activation mechanism, *Carbon*, **41**, 2 (2003) 267–275.

[16] S.-H. Yoon, S. Lim, Y. Song, Y. Ota, W. Qiao, A. Tanaka, I. Mochida, KOH activation of carbon nanofibers, *Carbon*, **42**, 8–9 (2004) 1723–1729.

[17] E. Yagmur, M. Ozmak, Z. Aktas, A novel method for production of activated carbon from waste tea by chemical activation with microwave energy, *Fuel*, **87**, 15–16 (2008) 3278–3285.

[18] A. H. Basta, V. Fierro, H. El-Saied, A. Celzard, 2-Steps KOH activation of rice straw: An efficient method for preparing high-performance activated carbons, *Bioresour. Technol.*, **100**, 17 (2009) 3941–3947.

[19] J. Xue, L. Huang, F. Jin, Qu. Liu, G. Liu, M. Wang, G. Li, S. Zhou, Two novel and simple strategies for improvement of the traditional activation method for activated carbon preparation: nano-copper catalysis and Cu(II) doping, *RSC Adv.*, **5** (2015) 81857–81865.

[20] Y. Yu, H.-S. Kil, K. Nakabayashi, S.-H. Yoon, J. Miyawaki, Toward development of

activated carbons with enhanced effective adsorption amount by control of activation process, *AIP Conf. Proc.*, **2097** (2019) 020002.

[21] N. Shiratori, K. J. Lee, J. Miyawaki, S.-H. Hong, I. Mochida, B. An, Pore structure analysis of activated carbon fiber by microdomain-based model, *Langmuir*, **25**, 13 (2009) 7631–7637.

[22] D.-W. Kim, H.-S. Kil, K. Nakabayashi, S.-H. Yoon, J. Miyawaki, Structural elucidation of physical and chemical activation mechanisms based on the microdomain structure model, *Carbon*, **114** (2017) 98–105.

[23] H. Shimanoe, S. Ko, Y.-P. Jeon, K. Nakabayashi, J. Miyawaki, S.-H. Yoon, Shortening stabilization time using pressurized air flow in manufacturing mesophase pitch-based carbon fiber, *Polymers*, **11**, 12 (2019) 1911–1925.

[24] M. J. Antal, Jr, E. Croiset, X. Dai, C. DeAlmeida, W. S.-L. Mok, N. Norberg, High-yield biomass charcoal, *Energy Fuels*, **10**, 3 (1996) 652–658.

[25] R. Santamaría-Ramírez, E. Romero-Palazón, C. Gómez-de-Salazar, F. Rodríguez-Reinoso, S. Martínez-Saez, M. Martínez-Escandell, Influence of pressure variations on the formation and development of mesophase in a petroleum residue, *Carbon*, **37**, 2 (1999) 445–455.

[26] J. J. Manyà, M. A. Ortigosa, S. Laguarta, J. A. Manso, Experimental study on the effect of pyrolysis pressure, peak temperature, and particle size on the potential stability of vine shoots-derived biochar, *Fuel*, **133** (2014) 163–172.

[27] D. Agar, N. DeMartini, M. Hupa, Influence of elevated pressure on the torrefaction of wood, *Energy Fuels*, **30**, 3 (2016) 2127−2136.

[28] G. Zhou, W. Zhong, A. Yu, Y. Dou, J. Yin, Experimental study on characteristics of pressurized grade conversion of coal, *Fuel*, **234** (2018) 965–973.

[29] W. Zhang, S. Sun, Y. Zhao, Z. Zhao, P. Wang, D. Feng, P. Li, Effects of total pressure and CO_2 partial pressure on the physicochemical properties and reactivity of pressurized coal char produced at rapid heating rate, *Energy*, **208** (2020) 118297.

[30] Q. Yan, J. Huang, J. Zhao, C. Li, L. Xia, Y. Fang, Investigation into the kinetics of pressurized steam gasification of chars with different coal ranks, *J. Therm. Anal. Calorim.*, **116**, 1 (2014) 519–527.

[31] I. Sircar, A. Sane, W. Wang, J. P. Gore, A study of high pressure pinewood char gasification with CO_2, *Fuel*, **134** (2014) 554–564.

[32] L. Liu, Q. Liu, Y. Cao, W.-P. Pan, The isothermal studies of char-CO_2 gasification using the high-pressure thermo-gravimetric method, *J. Therm. Anal. Calorim.*, **120**, 3 (2015) 1877–1882.

[33] Z. Liu, Q. Wang, Kinetic study on metallurgical coke gasification by steam under various pressures, *J. Therm. Anal. Calorim.*, **129**, 3 (2017) 1839–1845.

[34] X. Wu, J. Wang, K_2CO_3-catalyzed steam gasification of ash-free coal char in a pressurized and vertically blown reactor. Influence of pressure on gasification rate and gas composition, *Fuel Process. Technol.*, **159** (2017) 9–18.

[35] M. Tomaszewicz, G. Tomaszewicz, M. Sciazko, Experimental study on kinetics of coal char–CO_2 reaction by means of pressurized thermogravimetric analysis, *J. Therm. Anal. Calorim.*, **130**, 3 (2017) 2315–2330.

[36] W. Jiao, Z. Wang, X. Zhou, Y Mei, R. Feng, T. Liu, Catalytic steam gasification of sawdust char on K-based composite catalyst at high pressure and low temperature, *Chem. Eng. Sci.*, **205** (2019) 341–349.

[37] K. Kaneko, C. Ishii, M. Ruike, H. Kuwabara, Origin of superhigh surface area and microcrystalline graphitic structures of activated carbons, *Carbon*, **7**, 30 (1992) 1075–1088.

[38] A. V. Neimark, Y. Lin, P. I. Ravikovitch, M. Thommes, Quenched solid density functional theory and pore size analysis of micro-mesoporous carbons, *Carbon*, **47**, 7 (2009) 1617–1628.

[39] A. Ahmadpour, D. D. Do, The preparation of active carbons from coal by chemical and physical activation, *Carbon*, 34, 4 (1996) 471–479.

[40] J. A. Maciá-Agulló, B. C. Moore, D. Cazorla-Amorós, A. Linares-Solano, Activation of coal tar pitch carbon fibers: Physical activation vs. chemical activation, *Carbon*, **42**, 7 (2004) 1367–1370.

[41] F.-C. Wu, R.-L. Tseng, C.-C. Hu, Comparison of pore properties and adsorption performance of KOH-activated and steam-activated carbons, *Microporous Mesoporous Mater.*, **80**, 1–3 (2005) 95–106.

[42] B. Fathollahi, B. Jones, P. C. Chau, J. L. White, Injection and stabilization of mesophase pitch in the fabrication of carbon–carbon composites. Part III: Mesophase stabilization at low temperatures and elevated oxidation pressures, *Carbon*, **43**, 1 (2005) 143–151.

Chapter 5.

Application of pressurized physically activated carbon to ethanol adsorption heat pump

Study on the applicability of pressurized physically activated carbon as an adsorbent in adsorption heat pumps (H. Yi *et al.*, RSC Adv., **12** (2022) 2558–2563)

5.1 Introduction

Today, environmental friendliness, CO_2 emission reduction, thermal energy efficiency, and thermal management are important global concerns. A heat pump is a system capable of cooling, heating, and freezing by pumping heat. Heat pumps are widely used in homes and industrial plants. According to their drive power, heat pumps are classified into vapor compression (compressor), thermoelectric element (Peltier element), and absorption/adsorption types. Among these, the adsorption heat pump (AHP) is commercially available as adsorption type refrigerators. These refrigerators are equipped with a porous adsorbent and operate based on the adsorption cooling principle proposed by Faraday in 1848 [1]. Unlike other types of heat pumps, AHPs require almost no electricity for its operation and produces minimal vibration and noise. Furthermore, AHPs can be driven by solar heat or industrial low-temperature waste heat, preventing CO_2 emissions. Therefore, replacing existing heat pumps with AHPs can contribute to electric power saving and efficient waste thermal energy recycling. However, the large size of existing AHPs devices limits their widespread usage, necessitating the improvement of the performance of AHP systems.

Examples of AHP refrigerants include NH_3, water, alcohol, and CO_2 [2–4], while porous materials such as silica gel, synthetic zeolite, and activated carbon are used as adsorbents [5–7]. Synthetic zeolite–water is a commercial AHP adsorbent–refrigerant combination. Although water is inexpensive and safe, the zeolite–water pair is limited by low adsorption capacity, and water cannot obtain temperatures below ice point. Thus, activated carbon–ethanol has attracted increasing attention as an alternative pair [8–11]. For example, owing to its well-developed pore structure, activated carbon has a saturated ethanol-uptake capacity of 1900 mg/g [10]. Saturated ethanol uptake capacity is an important indicator of the maximum adsorption capacity of an adsorbent. Instead, "effective adsorption uptake" is used herein to denote the difference in adsorption uptake between adsorption and regeneration (desorption) conditions, as a critical index to assess the performance of AHP systems. This is because the AHP working pressure range is determined by the AHP operation temperatures (i.e., the temperatures of cooling water, the surrounding environment, and regeneration) and does not include the overall relative pressure (P/P_0) range of refrigerant (0–1). In a previous study, the AHP P/P_0 range was calculated as 0.1–0.3 of ethanol adsorption isotherms at 303 K under assumption of 283, 303, and 353 K for the cooling water, the surrounding environment, and regeneration temperatures, respectively. Under this condition, the maximum effective ethanol uptake occurred at a carbon pore slit width of 1.6 nm [12]. Chemically activated carbon with an average pore width of 1.6 nm showed a high effective ethanol uptake of > 700 mg/g [12].

However, conventional physical activation methods using atmospheric pressure CO_2 or steam cannot easily realize activated carbon with a large number of 1.6-nm micropores. In contrast, chemical activation using KOH or NaOH as the activation agent can introduce a large number of micropores and mesopores; however, the required post-treatment step of acid-washing and anti-corrosion equipment increase production costs. Thus, we recently developed a pressurized

physical activation method for activated carbon production [13]. The obtained activated carbon showed a high degree of pore development and characteristic pore size distribution, with a peak pore width of approximately 1.6 nm.

In this study, I investigated the applicability of pressurized physically activated carbon in AHP systems using ethanol refrigerant.

5.2 Experimental

5.2.1 Sample preparation

I used a carbonized BEAPS (C6) in the same manner as Chapters 3 and 4. C6 was activated at 900°C under CO_2 pressures of 0.1 MPa for 90 min and 1.0 MPa for 5 min to obtain atmospheric pressure and pressurized physically activated carbon, respectively. During chemical activation, a mixture of C6 and KOH (1:6 by weight) was heated to 900°C and held for 1 h under nitrogen flow. Afterward, washing, filtering, and drying were performed to obtain chemically activated carbon. Activated carbons obtained by atmospheric pressure activation (CO_2-activated carbon), pressurized physical activation (pressurized CO_2-activated carbon), chemical activation (KOH-activated carbon) are abbreviated as PAC, PPAC, and CAC respectively. Activation yield was calculated as follows:

$$\text{Activation yield}\,[\%] = 100[\%] - \text{Weight loss by activation process}\,[\%]$$

5.2.2 Adsorption measurements

Nitrogen adsorption–desorption isotherms at 77 K of the activated carbon prepared from C6 were obtained using a volumetric gas adsorption measurement device (Nova-e series; Anton Paar QuantaTec Inc., USA). Total pore volume and specific surface area were estimated through an α_S-plot analysis [14] of the N_2 adsorption isotherms. Average pore width was calculated using the estimated total pore volume and specific surface area, assuming a slit-shaped pore. Pore size distribution was obtained using the quenched solid density functional theory (QSDFT) method [15]. Micropore volume was calculated based on the size distribution of pores smaller than 2.0 nm. Porosity was calculated as

$$\text{Porosity}\left[\frac{\text{cm}^3}{\text{cm}^3}\right] = \text{Total pore volume}\left[\frac{\text{cm}^3}{\text{g}}\right] \times \text{Bulk density}\left[\frac{\text{g}}{\text{cm}^3}\right]$$

where bulk density was estimated by packing each specimen into a cylinder with 1.6-mm inner diameter and 2.5-mm length.

Ethanol adsorption–desorption isotherms at 303 K were obtained using a commercial volumetric adsorption apparatus (Belsorp-max; MicrotracBEL Corp., Japan).

5.2.3 Morphological characterizations

I determined particle size using a scanning electron microscope (SEM, JSM-6700F; JEOL, Japan) and evaluated the mean size of 300 particles in SEM images of each sample. To observe microdomain structure, scanning tunnelling microscope (STM, Agilent Technologies 5500 Scanning Probe Microscope; Toyo Corporation, Japan) images were also acquired using its constant current mode (current: 0.3–1.2 nA, bias voltage: 0.1–1.5 V, and scan frequency: 1–2 Hz).

5.2.4 Chemical characterizations

Raman spectra were obtained using a Laser Raman Microspectroscopy (Nanofinder® 30; Tokyo Instruments Inc., Japan) employing a 532 nm Ar-ion laser as the excitation source. Intensity ratio of D band and G band, I_D/I_G, was calculated from the peak intensities at 1350 cm^{-1} (D band) and 1580 cm^{-1} (G band) in the Raman spectra.

Elemental compositions of samples were analysed using a CHN analyzer (MT-6; Yanaco Analytical Systems Inc., Japan). The assay of O content ($O_{diff.}$) was defined by subtracting the

sum of the contents of C, H, and N from 100%.

5.3 Results and discussion

5.3.1 Pore structure of prepared samples

Figure 5-1 shows the N_2 adsorption–desorption isotherms at 77 K of starting carbonized material (C6), and the activated carbons derived via different activation methods. PAC showed Type I(a) isotherm, suggesting a presence of narrow micropores (of width < ~ 1 nm). PPAC and CAC showed Type I(b) isotherms, though a small Type H4 hysteresis loop was observed for CAC, according to the IUPAC classification [16]. This suggests that PPAC and CAC have pore size distributions over a broader range including wider micropores and possibly narrow mesopores. The activation yield and pore structural parameters of each activated carbon are summarized in **Table 5-1**. The specific surface area and total pore volume of C6 were 570 m^2/g and 0.21 cm^3/g, respectively. PAC showed an increased specific surface area of 1650 m^2/g and total pore volume of 0.60 cm^3/g. PPAC showed a comparable activation yield to PAC, but a much higher degree of pore development, with a specific surface area of 3290 m^2/g and total pore volume of 1.78 cm^3/g. Owing to chemical activation using KOH, CAC exhibited highly developed pores, with a specific surface area of 3010 m^2/g, total pore volume of 2.45 cm^3/g, and high activation yield of 31%. Chemically activated carbons are well known to exhibit higher activation yield and pore development than conventional physically activated carbons [17].

Table 5-2 presents bulk densities and porosities calculated from total pore volume and bulk density. PPAC showed the highest porosity (0.69 cm^3/cm^3), indicating effective pore development by pressurization. This high porosity was due to the high bulk density of PPAC (approximately twice that of CAC), although PPAC had a smaller total pore volume than CAC.

Figure 5-2 illustrates the pore size distributions calculated from the N_2 adsorption isotherms

at 77 K using the QSDFT method. Narrow micropores (< 1.0 nm) in C6 were presumably voids formed during the thermal decomposition of raw phenol resin. PAC, prepared by the atmospheric pressure physical activation method, developed numerous narrow micropores with pore widths of < 1.0 nm. Compared with PAC, CAC had fewer micropores smaller than 1.0 nm; however, it contained a large number of mesopores larger than 2.0 nm. In contrast, PPAC showed a characteristic bimodal pore size distribution, comprising narrow micropores smaller than 1.0 nm and wide micropores of approximately 1.6 nm. Pressurization enhanced the diffusibility of the activation agent (CO_2 gas) into carbon particles and induced the development of inter-microdomain pores [13]. Therefore, it was confirmed that the pressurized physical activation gave rise to the well-developed and unique pore structures between the atmospheric pressure physical activation and chemical activation methods.

5.3.2 Morphological characteristics

Figure 5-3 shows the SEM images and particle size distribution of starting material, C6, PAC, PPAC, and CAC. In addition, results of a heat-treated sample of C6 at 900°C in N_2 for 1 h (C6C9) are also shown in **Figure 5-3** for a comparison, because the activation process was carried out at 900°C. To all samples, spherical shape of particle was maintained. Any treatment at 900°C, that is, heat treatment in N_2, atmospheric and pressurized physical activations with CO_2, and chemical activation with KOH, induced a decrease of particle size. The mean particle size of CAC almost agreed with that of C6C9 (6.7 and 6.8 μm, respectively). On the other hand, PAC showed a noticeable decrease of mean particle size to 4.5 μm. PPAC gave the mean particle size of 5.8 μm; intermediate between PAC and CAC. This suggests that the diffusibility of the activation agent into carbon particles for the pressurized physical activation was between

the atmospheric pressure physical activation and chemical activation methods.

STM images of all activated carbon samples are shown in **Figure 5-4**. As reported in our previous works, inter-microdomain boundary suggests a development of inter-microdomain pores [13, 18]. PAC showed connected or unclear microdomain boundary. In contrast, PPAC and CAC showed clear inter-microdomain boundary. Moreover, CAC gave wider inter-microdomain gaps than PPAC. These results suggest that the wide pores including mesopores for CAC and the characteristic micropores of 1.6 nm for PPAC were originated from the inter-microdomain space.

5.3.3 Ethanol adsorption properties

Figure 5-5 shows ethanol adsorption–desorption isotherms measured at 303 K. Adsorption and desorption isotherms well overlapped each other for C6 and PAC, but PPAC and CAC showed small adsorption hysteresis loops at $P/P_0 > 0.4$. From these isotherms, both the saturated ($P/P_0 = 0.95$) and effective ($P/P_0 = 0.1–0.3$) adsorption uptakes of ethanol were estimated (**Table 5-4**). For C6, the non-activated carbon, the saturated adsorption uptake was small (170 mg/g), although the effective adsorption uptake was much smaller (10 mg/g). According to the pore structural parameters (**Table 5-1**) and pore size distribution (**Figure 5-2**), C6 possessed almost no pore structures that can contribute to the effective uptake of ethanol. The saturated uptake of ethanol by PAC was 730 mg/g, which was significantly higher than that by C6 (170 mg/g); however, the effective adsorption uptake was not so high enough (70 mg/g). This was because the pores developed via conventional atmospheric pressure physical activation were mainly narrow micropores (< 1.0 nm). Thus, PAC is not suitable as an adsorbent for AHP systems with ethanol refrigerant. Compared with PAC, CAC, with a high

degree of pore development, showed over eight times higher effective ethanol uptake (580 mg/g). PPAC achieved an effective ethanol uptake of 570 mg/g, comparable with that of CAC. The characteristic pore size distribution of PPAC, with an optimal pore size of 1.6 nm [12], provided high ethanol uptake at P/P_0 = 0.1–0.3 and thus showed the large effective adsorption uptake, despite its lower total pore volume than CAC. In addition, PPAC showed the highest effective ethanol uptake per unit volume of activated carbon (220 mg/cm^3; **Figure 5-6**, **Table 5-3**). In contrast, the value for CAC was only 120 mg/cm^3, because CAC contained a large number of wide pores, including mesopores, which contributed little to effective adsorption uptake. In other words, PPAC possessed "effective" pores. The superior volumetric ethanol adsorbability of PPAC suggests that it can improve AHP performance and reduce device size.

Furthermore, because of the post-treatment costs and expensive acid and alkali resistance equipment, chemical activation is much costlier than conventional atmospheric pressure physical activation. Although pressurized physical activation achieves a lower activation yield than chemical activation and requires a pressure-tight vessel, PPAC achieves a remarkably high effective ethanol uptake per unit volume; thus, it has potential as a relatively inexpensive, high-performance adsorbent for AHP systems with ethanol refrigerant.

5.3.4 Chemical properties

Raman spectroscopy (**Figure 5-7**) and elemental analysis (**Table 5-4**) were also carried out for confirming influence of functional groups on activated carbon for ethanol adsorption. However, relationships between the chemical properties and effective adsorption uptake of ethanol were not observed. As our research group have found that surface functional groups induced diffusional hindrance of ethanol molecules, giving rise to decreases of adsorption

uptake and shortening of adsorption equilibrium time of ethanol [19], detailed investigations on the influence of surface modification of PPAC on the ethanol adsorbability are important as future works.

5.4 Conclusion

In Chapter 5, I evaluated the applicability of pressurized physically activated carbon in AHP systems with ethanol refrigerant. The analyses of N_2 adsorption–desorption isotherms at 77 K revealed that the carbon prepared via pressurized physical activation exhibited wide micropores of approximately 1.6 nm. Such micropores were not observed in activated carbons prepared via conventional atmospheric pressure physical activation or chemical activation. The pressurized physically activated carbon showed high effective ethanol uptake on a weight basis. The uptake was comparable with that of chemically activated carbon, despite the large difference in total pore volume between both carbon materials. Moreover, the pressurized physically activated carbon exhibited a remarkably high effective ethanol uptake per unit volume. Therefore, the pressurized physically activated carbon has great potential as an adsorbent for AHP systems with ethanol refrigerant.

As future works, to realize the AHP systems of PPAC-ethanol pairs, I believe that adsorption-regeneration cycle tests are indispensable for a confirmation of the long-term stability.

Table 5-1. Activation yield and pore structural parameters of the starting carbonized material (C6) and derived activated carbons prepared by atmospheric and pressurized physical activation methods.

Sample	Activation pressure [MPa]	Activation yield [%]	Total pore volume [cm^3/g]	Micropore volume [cm^3/g]	Specific surface area [m^2/g]	Average pore width [nm]
C6	-	-	0.21	0.18	570	0.73
PAC	0.1	13	0.60	0.56	1650	0.73
PPAC	1.0	12	1.78	1.39	3290	1.09
CAC	0.1	31	2.45	1.01	3010	1.65

Table 5-2. Bulk density and porosity of starting carbonized material and derived activated carbons.

Sample	Bulk density [g/cm^3]	Porosity [cm^3/cm^3]
C6	0.84	0.18
PAC	0.57	0.35
PPAC	0.39	0.69
CAC	0.20	0.51

Table 5-3. Saturated and effective adsorption amounts of ethanol of starting carbonized material and derived activated carbons.

Sample	Saturated adsorption amount of ethanol [mg/g]	Effective adsorption amount of ethanol [mg/g]	Effective adsorption amount of ethanol [mg/cm^3]
C6	170	10	8
PAC	730	70	40
PPAC	1730	570	220
CAC	1630	580	120

Table 5-4. Elemental composition of starting carbonized material (C6), and the activated carbons derived via different activation methods (PAC, PPAC, and CAC).

Sample	C [wt.%]	H [wt.%]	N [wt.%]	$O_{diff.}$[wt.%]	Ash [wt.%]	$O_{diff.}$/C
C6	90.19	2.23	0.22	7.36	-	0.062
PAC	96.53	0.33	0.08	3.06	-	0.024
PAPC	93.66	0.34	0.09	5.91	-	0.047
CAC	95.15	0.02	0.14	4.69	-	0.037

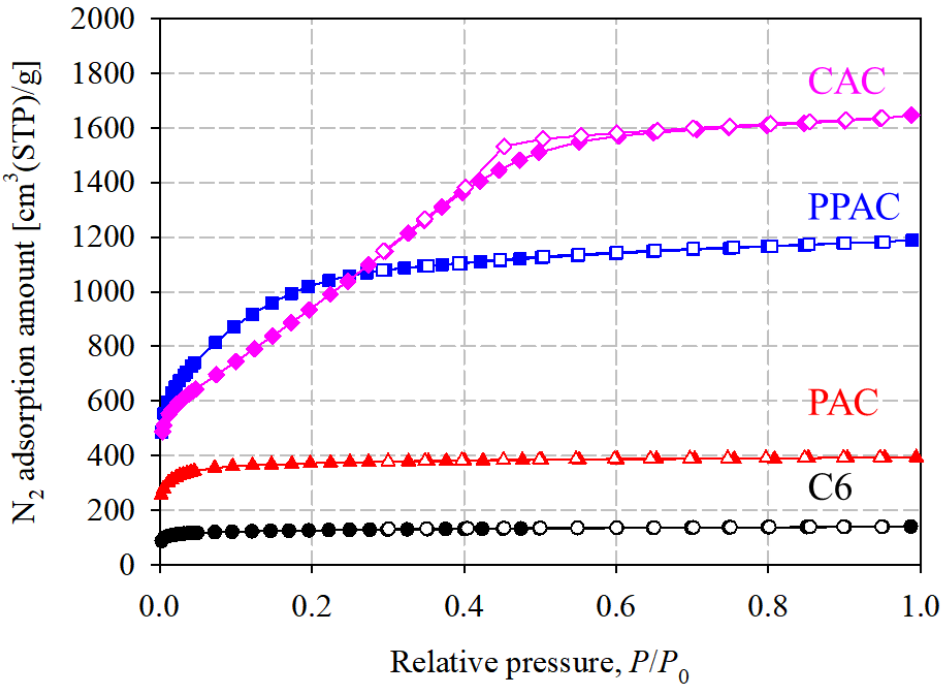

Figure 5-1. N_2 adsorption and desorption isotherms at 77 K of starting carbonized material (C6) and derived activated carbons prepared by different activation methods. Solid and open symbols denote adsorption and desorption isotherms, respectively. (Circle) C6; (Triangle) PAC; (Square) PPAC; (Diamond) CAC.

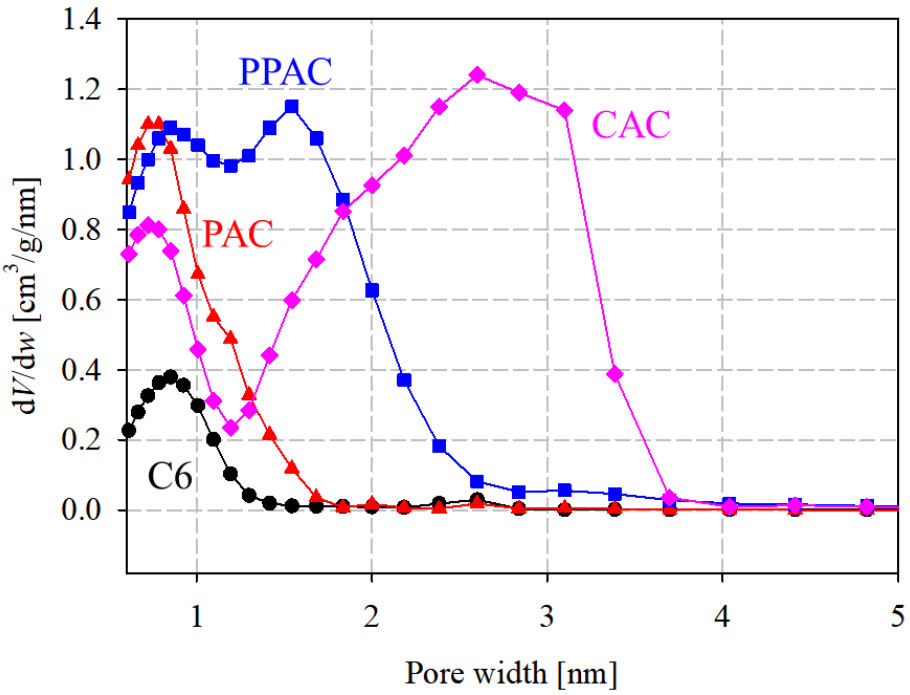

Figure 5-2. Pore size distributions for starting carbonized material and derived activated carbons. (Circle) C6; (Triangle) PAC; (Square) PPAC; (Diamond) CAC.

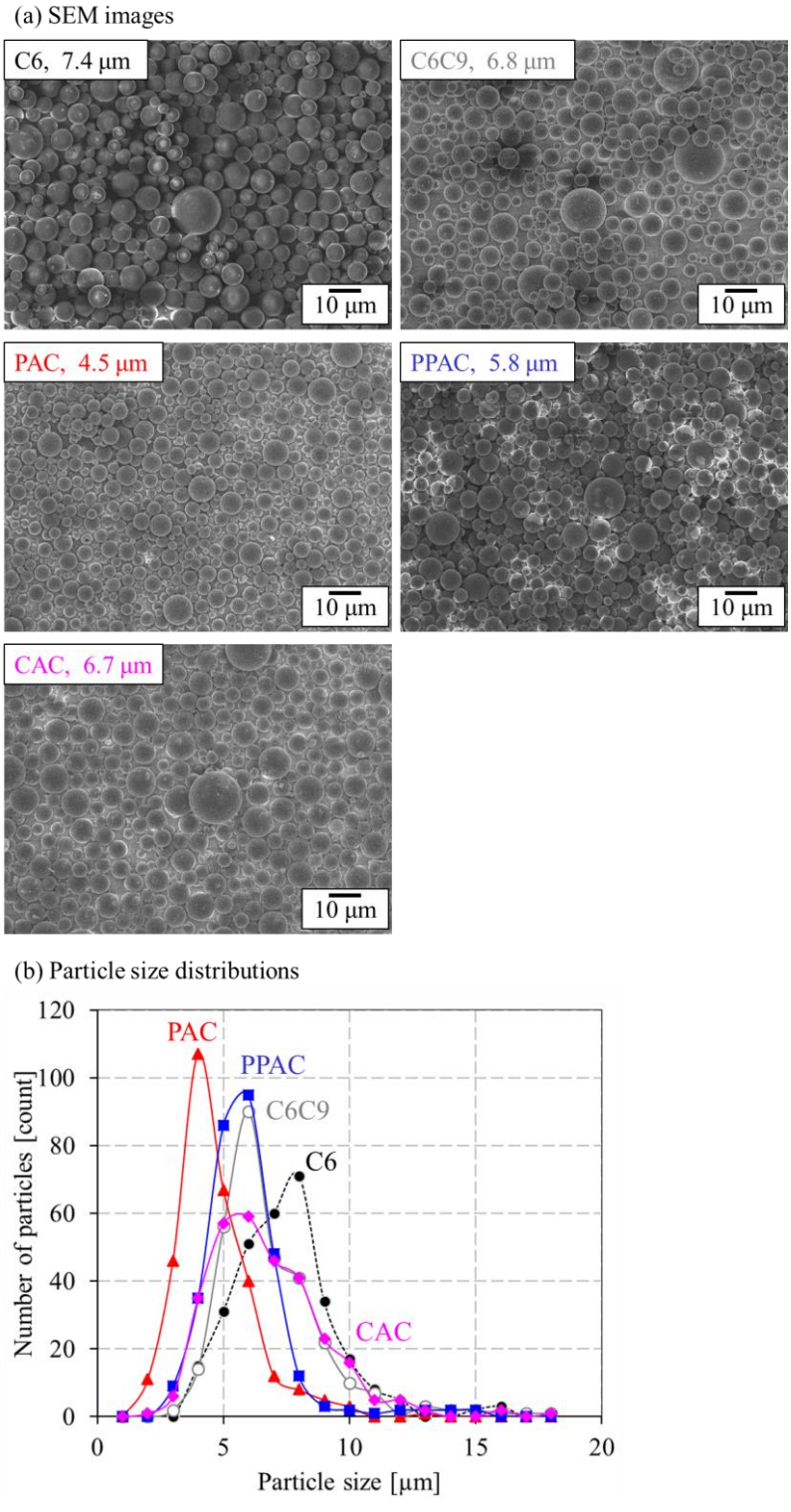

Figure 5-3. (a) SEM images and mean particle sizes and (b) particle size distributions of C6, C6C9, PAC, PPAC, and CAC.

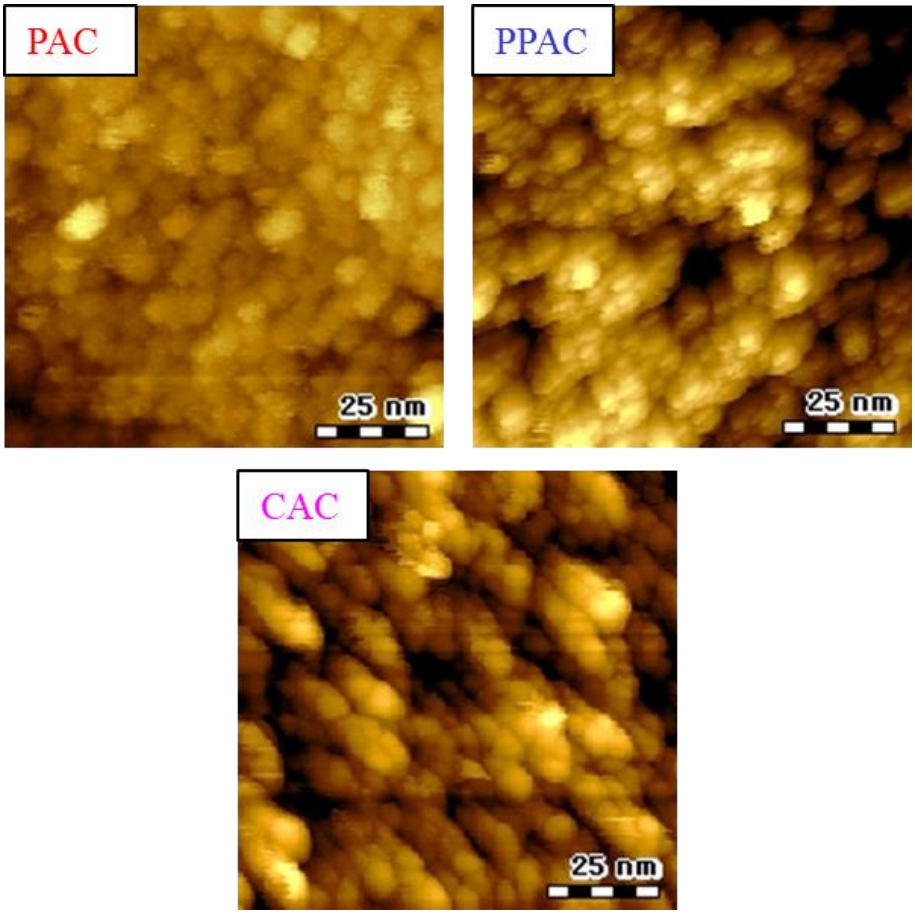

Figure 5-4. STM images of PAC, PPAC, and CAC.

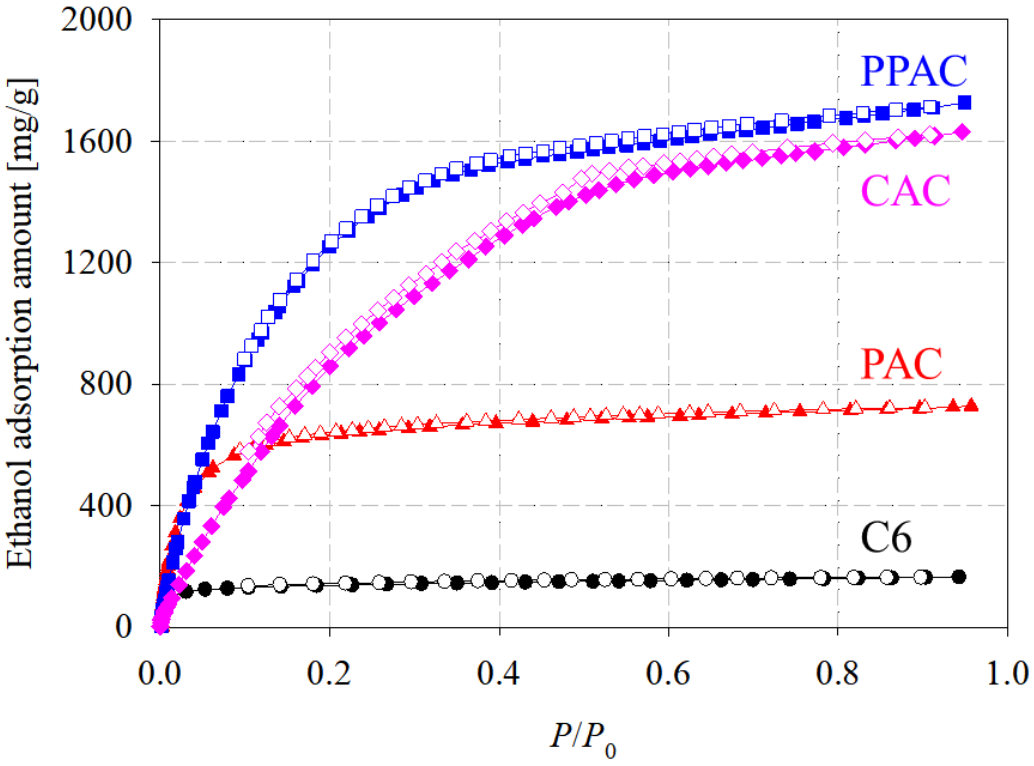

Figure 5-5. Ethanol adsorption–desorption isotherms at 303 K of starting carbonized material, and the derived activated carbons (circle: C6; triangle: PAC; square: PPAC; diamond: CAC).

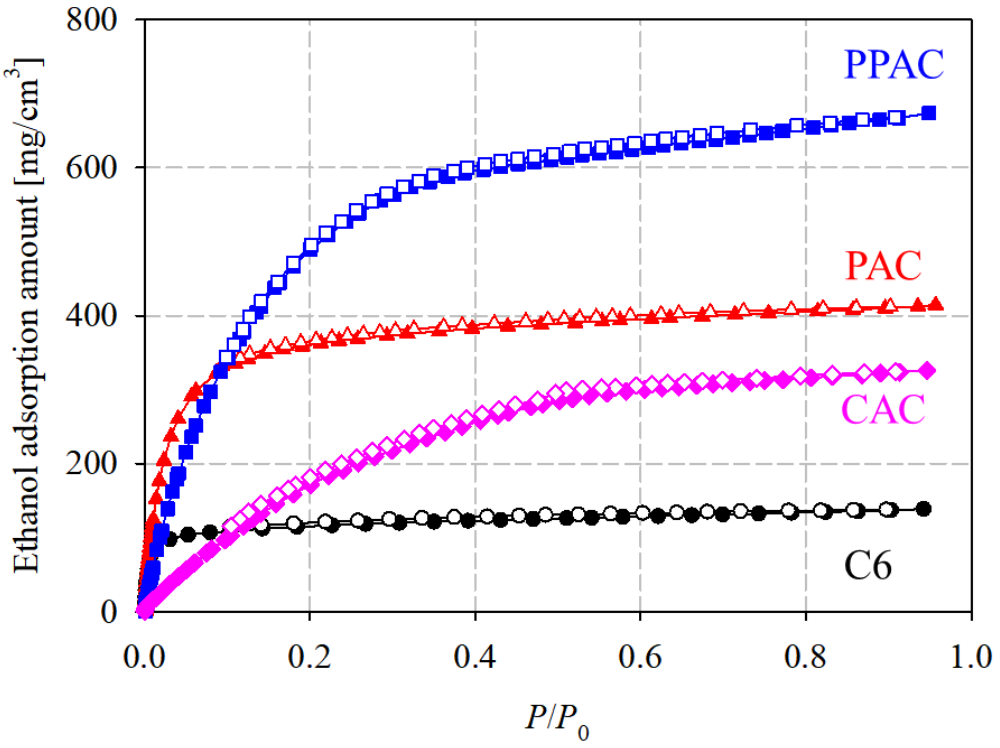

Figure 5-6. Ethanol adsorption–desorption isotherms on an adsorbent volume basis at 303 K of starting carbonized material, and the derived activated carbons. (circle: C6; triangle: PAC; square: PPAC; diamond: CAC).

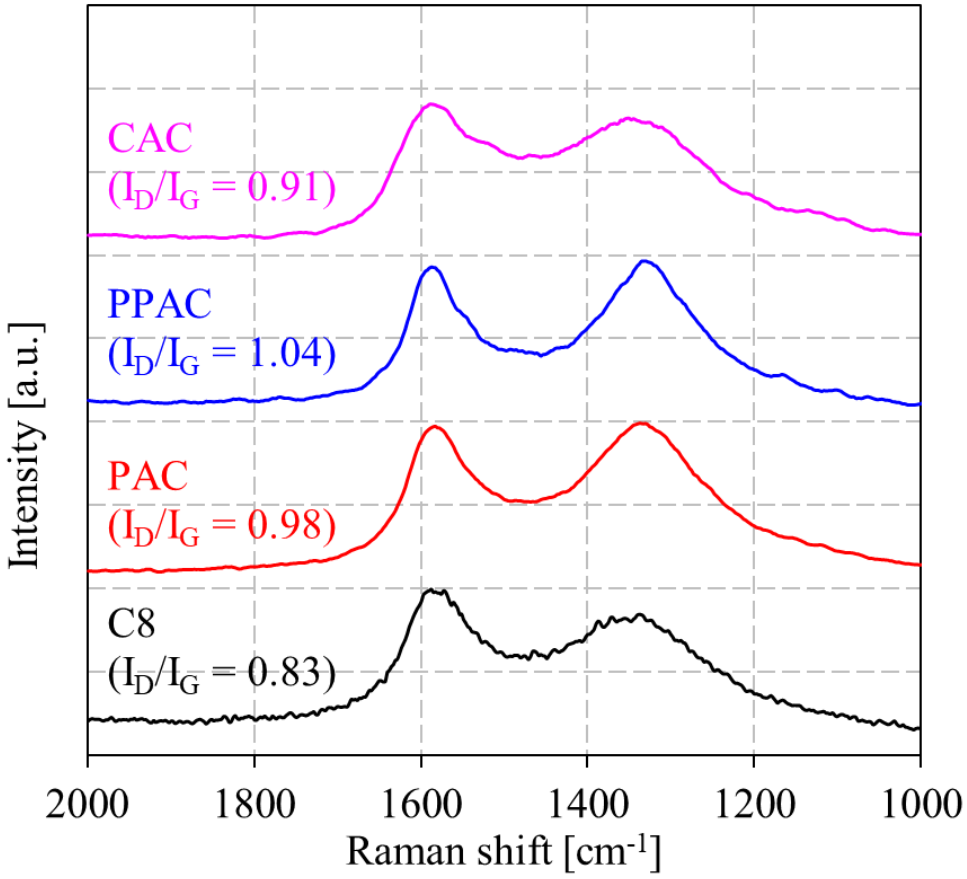

Figure 5-7. Raman spectra of starting carbonized material (C6), and the activated carbons derived via different activation methods (PAC, PPAC, and CAC).

References

[1] M. Faraday, XVII On the condensation of several gases into liquids, *Philosophical Transactions of the Royal Society of London*, **113** (1823) 189.

[2] D. -W. Sun, COMPARISON OF THE PERFORMANCES OF NH_3–H_2O, NH_3–$LiNO_3$ AND NH_3–NaSCN ABSORPTION REFRIGERATION SYSTEMS, *Energy Convers. Mgmt.*, **39** (1997) 357–368.

[3] E. E. Anyanwu, Review of solid adsorption solar refrigerator I: an overview of the refrigeration cycle, *Energy Convers. Mgmt.*, **39** (2003) 301–312.

[4] K. Nawaz, B. Shen, A. Elatar, V. Baxter, O. Abdelaziz, Performance optimization of CO_2 heat pump water heater, *Int. J. Refrigeration*, **85** (2018) 213–228.

[5] M. A. Tahat, Heat-pump/energy-store using silica gel and water as a working pair, *Appl. Energy*, **69** (2001) 19–27.

[6] J. Fukai, A. T. Wijayanta, Potential ability of zeolite to generate high-temperature vapor using waste heat, *AIP Conf. Proc.*, **1931** (2018) 020001.

[7] T. Kawano, M. Kubota, M. S. Onyango, F. Watanabe, H. Matsuda, Preparation of activated carbon from petroleum coke by KOH chemical activation for adsorption heat pump, *Appl. Therm. Eng.*, **28** (2008) 865–871.

[8] I. I. El-Sharkawy, B. B. Saha, S. Koyama, J. He, K.C. Ng, C. Yap, Experimental investigation on activated carbon–ethanol pair for solar powered adsorption cooling applications, *Int. J. Refrigeration*, **31** (2008) 1407–1413.

[9] K. Uddin, I. I. El-Sharkawy, T. Miyazaki, B. B. Saha, S. Koyama, H. -S. Kil, J. Miyawaki, S. -H. Yoon, Adsorption characteristics of ethanol onto functional activated carbons with controlled oxygen content, *Appl. Them. Eng.*, **72**, 2 (2014) 211–218.

[10] A. Pal, K. Thu, S. Mitra, I. I. El-Sharkawy, B. B. Saha, H.-S. Kil, S.-H. Yoon, J. Miyawaki,

Study on biomass derived activated carbons for adsorptive heat pump application, *Int. J. Heat Mass Trans.*, **110** (2017) 110, 7–19.

[11] P. Huo, Y. Zhang, L. Zhang, M. Yang, W. Wei, X. Zhang, J. Yang, Y. Zhang, Insight into the Adsorption Process of Ethanol and Water on the Pore Structure and Surface Chemistry Properties Engineered Activated Carbon Fibers, *Ind. Eng. Chem. Res.*, **60**, 30 (2021) 11141–11150.

[12] T. Miyazaki, J. Miyawaki, T. Ohba, S.-H. Yoon, B. B. Saha, S. Koyama, Study toward high-performance thermally driven air-conditioning systems, *AIP Conf. Proc.*, **1788** (2017) 020002.

[13] H. Yi, K. Nakabayashi, S.-H. Yoon, J. Miyawaki, Pressurized physical activation: A simple production method for activated carbon with a highly developed pore structure, *Carbon*, **183** (2021) 735–742.

[14] K. Kaneko, C. Ishii, M. Ruike, H. Kuwabara, Origin of superhigh surface area and microcrystalline graphitic structures of activated carbons, *Carbon*, **7**, 30 (1992) 1075–1088.

[15] A. V. Neimark, Y. Lin, P. I. Ravikovitch, M. Thommes, Quenched solid density functional theory and pore size analysis of micro-mesoporous carbons, *Carbon*, **47**, 7 (2009) 1617–1628.

[16] M. Thommes, K. Kaneko, A. V. Neimark, J. P Oliver, F. Rodriguez-Reinoso, J. Rouquerol, K. S. W. Sing, Physisorption of gases, with special reference to the evaluation of surface area and pore size distribution (IUPAC Technical Report), *Pure Appl. Chem.*, **87** (2015) 1051–1069.

[17] D.-W. Kim, H.-S. Kil, K. Nakabayashi, S.-H. Yoon, J. Miyawaki, Structural elucidation of physical and chemical activation mechanisms based on the microdomain structure model, *Carbon*, **114** (2017) 98–105.

[18] N. Shiratori, K. J. Lee, J. Miyawaki, S.-H. Hong, I. Mochida, B. An, K. Yokogawa, J. Jang, S.-H. Yoon, Pore structure analysis of activated carbon fiber by microdomain-based model, *Langmuir*, **25**, 13 (2009) 7631–7637.

[19] H.-S. Kil, T. Kim, K. Hata, K. Ideta, T. Ohba, H. Kanoh, I. Mochida, S.-H. Yoon, J. Miyawaki, Influence of surface functionalities on ethanol adsorption characteristics in activated carbons for adsorption heat pumps, *Appl. Them. Eng.*, **72**, 2 (2014) 160–165.

Chapter 6.

General conclusion

To produce activated carbon having high yield and pore development degree by physical activation, I proposed pressurized physical activation method. Physical activation method can produce activated carbon with low cost, but the yield and pore development degree goes low too. In this thesis, I would like to suggest new method based on physical activation process. Based on previous works of our research group, I tried pressurization on physical activation process. By pressurized physical activation, I successfully produced activated carbon with high yield and high pore development degree. In addition, unique pore width was introduced by pressurization which developed in inter-microdomain structure. Also, I applied and evaluated pressurized activated carbon to ethanol adsorption heat pump as advanced device. As a consequence, pressurized activated carbon The conclusions of each chapters for pressurized physical activation method and its application results are summarized below;

Chapter 3. Effect and factors about pressurized activated carbon manufacturing process

In Chapter 3, to find and explain the factors by pressurization on the physical activation process, I tried physical gasification by MSB-TG. I confirmed the effect of pressure application on the gasification reaction with oxidizing gas, and examined the possibility of the pressurized physical activation method. The gasification reactivity of the carbonized spherical phenol resin was evaluated under pressurized conditions using MSB-TG. As a result, it was confirmed that

the gasification reaction occurred at a lower temperature due to the pressurization. Furthermore, it was confirmed that the temperature required to achieve the specific gasification rate was decreased by pressurization. It is considered that the pressurization improved the diffusibility of the activation agent gas and gasification reaction, similar to the result seen in the pressurized stabilization in the carbon fiber manufacturing process in our previous study. In addition, as a result of evaluating the pore structure of activated carbon produced by atmospheric / pressurized physical activation using MSB-TG, it was confirmed that the specific surface area was greatly improved and the pore size distribution was also significantly changed by pressurization. As a result of observing the microdomains of each sample, a difference in microdomain size was observed, which is presumed to be the cause of the change in the pore structure due to pressurization. On the other hand, since almost no change in the size of the particles was observed even when pressurized, it is considered that uniform activation was performed inter- and intra-particle level. From these results, it was possible to confirm the effect of pressurized physical activation on the factors of activated carbon such as the yield of activated carbon, pore structure, particles and microdomains.

Chapter 4. Effect of pressurization on activated carbon manufacturing process

To produce activated carbon with a highly developed pore structure by a simple production process, I proposed a novel pressurized physical activation method. I found that this pressurized activated carbon achieves either a higher degree of pore development for a similar activation yield or a higher activation yield for a similar degree of pore development. Furthermore, a characteristic pore size distribution, with a maximum at approximately 1.6 nm, was obtained

by pressurization. Observations of particles and microdomains revealed that pressurization improved the activating agent diffusibility in carbon particles, but not in their microdomains. Consequently, I have successfully demonstrated the effectiveness of the pressurized physical activation method to produce activated carbon with a high degree of pore development by means of improving activating agent diffusibility at the particle level.

Chapter 5. Application of pressurized physically activated carbon to ethanol adsorption heat pump

In Chapter 5, I evaluated the applicability of pressurized physically activated carbon in adsorption heat pump systems with ethanol refrigerant. The analyses of N_2 adsorption–desorption isotherms at 77 K revealed that the carbon prepared via pressurized physical activation exhibited wide micropores of approximately 1.6 nm. Such micropores were not observed in activated carbons prepared via conventional atmospheric pressure physical activation or chemical activation. The pressurized physically activated carbon showed high effective ethanol adsorption amount on a weight basis. The uptake was comparable with that of chemically activated carbon, despite the large difference in total pore volume between both carbon materials. Moreover, the pressurized physically activated carbon exhibited a remarkably high effective ethanol adsorption amount per unit volume. Therefore, the pressurized physically activated carbon has great potential as an adsorbent for adsorption heat pump systems with ethanol refrigerant.

As a consequence of this thesis, I can confirmed the effect of pressurization on physical activation process. The pressurization on physical activated carbon manufacturing process, it can produce high yield and high pore development degree on activated carbon with lower cost. In the not-so-far future, I expect that the physical activated carbon manufacturing method by pressurization as facile and effective activated carbon manufacturing process, can contribute to reducing manufacturing costs and improving device performance.

本論文の要約、まとめ

活性炭は石炭、石油、高分子樹脂、バイオマス等の原料から作られる炭素化物に発達した細孔構造を付与した機能性炭素材料である。その発達した細孔構造のため活性炭は大きな比表面積を有し、分子やイオン等の吸着質の濃度が周りの環境よりも固体表面で高くなる吸着現象によって高い表面機能性を発現する。この表面機能性を活かし活性炭は従来から様々な分野で幅広く使用されているが、近年は先端デバイスへの適用も注目されており、より高い細孔発達度の高性能活性炭が求められている。炭素材料に細孔構造を付与する工程である賦活は、化学賦活と物理賦活に大別される。化学賦活は高細孔発達度の活性炭の高収率製造が可能であるが、賦活剤の値段、特殊設備や後処理工程が活性炭の製造コストの高騰をもたらしている。一方、物理賦活は安価に活性炭を製造できる方法であるが、付与できる細孔発達度に限界があり、収率も低いという課題がある。そのため、「化学賦活法のような高細孔発達度」の活性炭を、「物理賦活法のような安価な工程」で、高収率製造できる新規手法の開発が求められている。

新しい高性能活性炭製造法として、１）マイクロドメイン構造モデルに基づいた炭素材料の階層的構造モデルと細孔構造の関係性、２）従来の物理賦活法における低収率および低細孔発達度は賦活剤（酸化性ガス）の炭素材料内部における拡散性の低さに起因すること、そして、３）圧力印加によるガスの炭素材料内部における拡散性の向上、と言う３つの先行研究に基づき、本研究では加圧物理賦活法を提案する。加圧物理賦活法の有効性を確認すべく、まず圧力印加による炭素材料のガス化特性への影響を把握し、続いて実際に加圧物理賦活法を適用して活性炭を調製し、その細孔構造評価を試みた。さらに、加圧物理賦活法により調製した高細孔発達度活性炭の先端デバイスへの応用可能性について検討を行った。

本論文の各章の内容は以下のようにまとめる。

第1章では、活性炭の製造方法と細孔構造モデルについて紹介し、本研究における目的と手法を示した。

第2章では、活性炭に代表される多孔性炭素材料の各種分析・解析手法について述べた。

第3章では、加圧物理賦活のシミュレーション的検討として、高圧熱重量分析装置を用いて圧力印加下における炭素材料のガス化特性を評価し、さらに得られた加圧物理賦活炭の試作品の細孔構造を調べた結果を報告した。まず、加圧によって、炭素粒子のガス化反応が促進することを確認した。次に、反応温度を調整することで、印加圧力は異なるものの賦活収率（ガス化収率）が同程度の活性炭を試作した。これらの活性炭の細孔構造を評価した結果、印加圧力が

高くなるに連れ、細孔構造が発達する傾向が確認でき、特徴的な細孔径を付与できることを見出した。さらに、圧力印加によって細孔発達度が向上したのにもかかわらず、炭素粒子径はほとんど変わらない一方で、炭素粒子の基本構造単位（マイクロドメイン）のサイズは減少したことから、加圧によって賦活剤（CO_2ガス）の拡散性が向上し、炭素粒子内部へ賦活剤が効果的に浸透して、炭素粒子中心部においてもマイクロドメイン内およびマイクロドメイン間細孔が発達することを明らかにした。

第4章では、作製した管状反応炉を用いて加圧物理賦活法により活性炭を製造し、常圧物理賦活炭との差異について考察を行った。賦活時間や温度を調整し異なる賦活度の常圧および加圧物理賦活炭を調製した。これらの活性炭を評価した結果、加圧物理賦活法では従来の常圧物理賦活法では達成が困難な2,600 m^2/g以上の比表面積を達成できることを見出した。さらに、加圧物理賦活炭は1.6 nm付近にピークを持つ特徴的な細孔径分布を示すことを確認した。また、（活性炭重量当たりおよび炭素化物重量当たりの）細孔発達度、そしてかさ密度および空隙率に対する賦活収率の相関検討に基づき、加圧により細孔発達に寄与しない無駄なガス化反応が抑制され、加圧物理賦活炭の高収率と高細孔発達度をもたらされることを示した。加えて、炭素粒子およびマイクロドメイン観察の結果、常圧物理賦活においては賦活度が高くなるに連れて粒子径と分布が縮小する一方で加圧物理賦活炭では賦活度が高くなっても粒子径が維持されること、マイクロドメインは圧力印加によって縮小することが明らかになった。これらの結果から、加圧物理賦活炭の高細孔発達度と特徴的な細孔径分布は、マイクロドメイン間に生じた細孔由来である可能性を示した。

第5章では、加圧物理賦活法で製造した高細孔発達度・高収率の活性炭を先端デバイスの一種である吸着式ヒートポンプへ応用した効果について報告した。加圧物理賦活法によって活性炭ーエタノール型吸着式ヒートポンプとして適した細孔径1.6 nmの細孔を選択的に導入できたため、加圧物理賦活炭は、活性炭単位重量当たりのエタノール有効吸着量は化学賦活炭とほぼ同程度、単位体積当たりエタノール有効吸着量は常圧物理賦活炭の5倍以上、化学賦活炭の2倍近い高い性能を示した。加圧物理賦活炭による性能改善は、装置の小型化への寄与と共に、安価な方法で高細孔発達度の活性炭の製造ができるため、装置の低価格化ももたらすと期待される。

第6章では、加圧物理賦活法についてこれまでの成果と今後の展開について総括した。

Acknowledgement

I would like to express my special thanks to Prof. Jin Miyawaki, Prof. Seong-Ho Yoon, and Prof. Koji Nakabayashi for not only supervising my research and doctoral course but also guiding when I lost my way what I have to do. Without your help, I'm sure that I would never have earned Ph. D. degree in my life. I will keep continue your research philosophy and mind.

I would like to appreciate to Prof. Kazuhiko Miyazaki for advice and comments in my Ph. D. defense. I can contact to new field and viewpoint of my research because of his comments and papers.

I would like to thanks to group members in Yoon & Miyawaki laboratory for their help and cooperation during my graduate and doctoral course, particularly, Takaaki Shimohara as visiting professor, Ms. Miho Nakano as secretary in laboratory, Dr. Hiroki Shimanoe as fellow and supporter when I arrived in Japan first time, Dr. Islam MD Amirul, Mr./Miss Takashi Mashio, Kohei Ono, Yuto Tanaka, Shuo Cao, Ryo Sakai, Saki Nishida, Yasuhiro Koshi, Takaya Tokumaru, Taisei Tomaru, Shota Nishi, Yuanshuo Peng, Minghao Li, Kenta Morinaga. I would like to say thank you additionally to Mr. Sho Yoshida and Takuya Ito as my same period in graduate course. I wish your success what you do everything.

I’m deeply grateful to Korean fellows in our laboratory, particularly, Dr. Hyun-Sig Kil, Dr. Doo-Won Kim as not only fellow but also friend, Dr. Dong-Yeon Ryu, Ms. Dabin Chung, Mr. Minki Sung as same period of doctoral course. I will never forget every moment of us. I want to meet you all again not far future.

I would like to thank ASAHI YUKIZAI Co., Ltd. for providing samples for this research. I also would like to thank all the other people who have helped me in research and study abroad

life.

Finally, dear my family; father, mother, and my sister. I can achieve Ph. D. degree in Japan from your support and sacrifice. Thank you so much and I love you forever.

March, 2022

Hyeonseok Yi